KUOPION YLIOPISTON JULKAISUJA C. LUONNONTIETEET JA YMPÄRISTÖTIETEET 266
KUOPIO UNIVERSITY PUBLICATIONS C. NATURAL AND ENVIRONMENTAL SCIENCES 266

SALVATORE DI GIROLAMO

Sensing of Multimode Optic-Fiber Dynamic Strains by Using Self-Adaptive Holographic Interferometers

Doctoral dissertation

To be presented by permission of the Faculty of Natural and Environmental Sciences of the University of Kuopio for public examination in Auditorium ML1, Medistudia building, University of Kuopio, on Friday 18th December 2009, at 10 a.m.

Department of Physics
University of Kuopio

KUOPION YLIOPISTO

KUOPIO 2009

Distributor: Kuopio University Library
P.O. Box 1627
FI-70211 KUOPIO
FINLAND
Tel. +358 40 355 3430
Fax +358 17 163 410
http://www.uku.fi/kirjasto/julkaisutoiminta/julkmyyn.shtml

Series Editors: Professor Pertti Pasanen, Ph.D.
Department of Environmental Science

Professor Jari Kaipio, Ph.D.
Department of Physics

Author's address: Department of Physics
University of Kuopio
P.O. Box 1627
FI-70211 KUOPIO
FINLAND
Tel. +358 505502195
E-mail: girolamo@messi.uku.fi, digirosalvo@tiscali.it

Supervisors: Professor Alexei Kamshilin, Dr.Sc.
Department of Physics, University of Kuopio

Professor Pasi Karjalainen, Ph.D.
Department of Physics, University of Kuopio

Reviewers: Dr. Konstantin Shchebin, Senior Researcher
Institute of Physics, Kiev, National Academy of Sciences of Ukraine

Dr. Armin Kiessling,
Fraunhofer Institute For Applied Optics and Precision Engineering IOF
Friedrich Schiller University of Jena, Germany

Opponent: Professor Timo Jääskeläinen, Ph.D.
Department of Physics and Mathematics
University of Joensuu, Finland

ISBN 978-951-27-1404-9
ISBN 978-951-27-1299-1 (PDF)
ISSN 1235-0486

Kopijyvä
Kuopio 2009
Finland

Di Girolamo, Salvatore. Sensing of multimode optic-fiber dynamic strains by using self-adaptive holographic interferometers.
Kuopio University Publications C. Natural and Environmental Sciences 266. 2009. 53 p.
ISBN 978-951-27-1404-9
ISBN 978-951-27-1299-1 (PDF)
ISSN 1235-0486

ABSTRACT

Two-wave mixing (TWM) via a dynamic hologram recorded in a photorefractive crystal allows the implementation of adaptive interferometers. These interferometers can achieve high sensitivity of detection of phase shifts under unstable environmental conditions even when phase shifts are encrypted in speckled waves such as those reflected from rough surfaces or emerging from multimode optical fibers. Such abilities find potential applications in the field of vibration sensing for industrial, military and other purposes.

In this thesis we present three novel configurations for adaptive interferometers which are based on the vectorial wave mixing (VWM) technique in a CdTe photorefractive crystal. The WVM is a special case of the TWM in which the mixing of light waves in the photorefractive crystal involves different polarization states of waves in order to achieve linear phase-to-intensity transformation and the highest SNR. We have developed those configurations for the detection of multimode fiber strain induced by mechanical vibrations.

Two of these configurations use the reflection and orthogonal geometry of hologram recording respectively and each of them employs a single multimode optical fiber as a sensitive element. It is shown that the reflection geometry of hologram recording is characterized by a better combination of detection limit and adaptability than the transmission geometry which is more commonly used. We have found that the installation of a polarizer, which is needed in any classical configuration of TWM, results in the appearance of a strong noise. Such a noise, which we term polarization noise, relates to the polarization instability of the dynamic speckle pattern emerging from the fiber, which cannot be compensated for by the dynamic hologram. However, it has been demonstrated that this noise can be diminished by using an optical fiber with a larger core. The orthogonal geometry of hologram recording allows the linear regime of the phase-to-intensity transformation even when phase shifts are encrypted in a depolarized wave without using any polarizing element. Using a depolarized beam without a polarizing element strongly diminishes the level of the noise related to instabilities in the speckle pattern emerging from multimode optical fiber, thus increasing the sensitivity to phase transients. The third configuration represents a multiplexing scheme for sensing dynamic strains excited in different multimode optical fibers. The multiplexing of the sensors is implemented by using the vectorial wave mixing technique in the reflection geometry of hologram recording. For this configuration it is shown that we can minimize the crosstalk between the channels by choosing the appropriate crystallographic orientation that the interfering beams travels through. Moreover, we analyzed the physical mechanisms which lead to the appearance of the noise between the measuring channels in this configuration.

PACS Classification: 42.25.Hz, 42.40.Pa, 42.40.Ht, 42.40.Kw, 42.65.Hw, 42.81.Pa, 42.40.Lx, 46.40.-f
Universal Decimal Classification: 531.715, 534.1, 535.41, 681.7.068, 778.38
INSPEC Thesaurus: light interference; holography; interferometers; interferometry; holographic interferometry; photorefractive effect; photorefractive materials; crystals; light polarisation; multiwave mixing; speckle; optical fibres; fibre optic sensors; strain sensors; vibrations; optical noise; optical crosstalk

ACKNOWLEDGMENTS

This study was carried out at the Department of Physics, University of Kuopio, during 2005-2009. The study was supported by the Academy of Finland under project number 14102.

I wish to express my gratitude to my supervisor, Prof. Alexei Kamshilin, for his professional guidance in this research field, for his inspiration and encouragement at all times.

I would like to take this opportunity to thank Dr. Roman Romashko and Dr. Ervin Nippolainen, whose professionalism and experience in optics greatly improved the results and quality of my research.

I am also indebted to all the staff of the Department of Physics with whom I have been in contact, and to many others at the University of Kuopio for rendering help and providing a positive working environment. I am especially grateful to Vivian Paganuzzi, MA, of the Language Centre, for his help in improving the language of my scientific texts.

My deepest gratitude goes to my family, for their constant support and patience while I was working on my research

LIST OF ORIGINAL PUBLICATIONS

The thesis includes the conducted research review based on the peer-reviewed original papers written by the author and devoted to the research field. The original papers are referred to by their Roman numerals:

I. S. Di Girolamo, A. A. Kamshilin, R. V. Romashko, and Y. N. Kulchin, "Fast adaptive interferometer on dynamic reflection hologram in CdTe:V," Optics Express **15,** 545-555 (2007).

II. S. Di Girolamo, A. A. Kamshilin, R. V. Romashko, Y. N. Kulchin, and J.-C. Launay, "Sensing of multimode-fiber strain by dynamic photorefractive hologram," Optics Letters **32,** 1821-1823 (2007).

III. Romashko, S Di Girolamo, Y N Kulchin1, J C Launay, and A A Kamshilin, "Fast-adaptive fiber-optic sensor for ultra-small vibration and deformation measurement," Journal of Physics: Conference Series **85** (2007) 012024.

IV. R. Romashko, Y. Kulchin, S.D. Girolamo, A. A. Kamshilin and J.C. Launay, "Adaptive Fiber-Optical Sensor System for Pico-Strain and Nano-Displacement Metrology", Engineering Materials, **381-382,** 61-64, (2008).

V. S. Di Girolamo, R. V. Romashko, Y. N. Kulchin, J.-C. Launay, and A. A. Kamshilin, "Fiber sensors multiplexing using vectorial wave mixing in a photorefractive crystal," Optics Express, **16**, no. 22, 18041-18049, (2008).

VI. S. Di Girolamo, A. A. Kamshilin, R. V. Romashko, Y. N. Kulchin, and J.-C. Launay, "Orthogonal geometry of wave interaction in a photorefractive crystal for linear phase demodulation", Optics Communications, **283,** 128-131, (2010).

VII. S. Di Girolamo, A. A. Kamshilin, R. V. Romashko, Y. N. Kulchin, and J.-C. Launay, Photorefractive Vectorial Wave Mixing in Different Geometries, (submitted to the Journal of the Optical Society of America B).

Contents

Chapter 1

Introduction

When a source creates sound in media like metal, liquid, gas, etc, there will be energy transfer of mechanical energy from the source to the adjacent molecules. The energy travels through the media by compression and expansion of outlying molecules in it. Such behavior is generally described by the physical model of the sounds waves. Usually, conventional transducers convert the mechanical energy of a sound wave into an electrical. However, because of their nature, such systems are sensitive to electromagnetic fields which can influence the electric signal travelling in metallic cables. Moreover, the electrical signal produced by the transducer has to be enhanced by a pre-amplifier installed close to the transducer.

Fiber optics represents an alternative and simpler way to implement transducers. Fiber optics sensors does not convert directly acoustical waves into electrical signals as it happens with conventional transducers, but instead they convert first the sound in changes of the intensity or of the phase of light travelling through the optical fiber. For example, during operation in fiber optic microphones, light from a laser source travels through an optical fiber to illuminate the surface of a thin diaphragm which is sensitive to the sound and which is reflective to the light. The light which is reflected from the diaphragm is partially collected by another optical fiber. When impact of the sound wave let the diaphragm vibrate, the mechanical displacements of the diaphragm shift the position of the reflected light, thus changing the intensity of the light collected by the second fiber. The intensity modulation of the transmitted light traveling in the second fiber is afterwards sent to a photodetector.

Optical fiber sensors show specific advantages with respect conventional transducers. Their advantages relates with the physical nature of light propagation in the optical fiber; no metal parts, a less time consuming, no electric power is needed, immunity from electromagnetic fields and listed a few. Due to the low light losses in optical fiber, the distance between sensor, light source and photodetector may be up to several kilometers.

Optical fibers are not used only for conveying light but they can also be used as sensors for detection of many physical parameters (i.e temperature, pressure, sound waves, etc). The impact of sound waves on the optical fiber induces fiber strains and consequently change the length of the path in which the light travels. Consequently, changes of the path in which light travels are transferred in variations of the phase of the light wave emerging from fiber's output. When the light traveling in the optical fiber is originated by a highly coherent source (i.e. laser), high sensitivity of phase

detection can be achieved by using an interferometer. However, the detection of phase shifts from optical fiber is not an easy task when a classical interferometer is employed.

Classical interferometers operate a phase-to-intensity transformation only by combining the objet wave containing the phase modulation with a reference wave. Fiber optic sensors usually employ the single mode optical fiber although the multimode fiber (MMF) represents a better solution for a stable coupling with the light source. The reason is that classical interferometers do not ensure highly visible interference with the reference wave when the object wave has a speckled wavefront like that emerging from MMF. Another problem for classical interferometers is the stabilization of the working point under unstable environmental conditions. A stable working point is necessary to preserve in time the linear regime of the detection of phase shifts. It is well known that the linear regime of the phase-to-intensity transformation is achieved when a phase difference of $\pi/2$ radians exists between the object wave and the reference wave. However, slow time-varying environmental parameters like temperature or pressure affect the optical fiber for all its length, thus inducing slow phase changes with magnitude much bigger than phase changes induced by sound waves (i.e. ultrasounds). Such big phase changes may strongly affect the averaged phase shift, thus shifting the position of the working point. Therefore, different electronic systems may be used to stabilize the interferometer.

The two-wave-mixing (TWM) is a technique that can be used for the implementation of self-adaptive interferometers which are able to detect phase changes encrypted in speckled waves such those reflected from rough surfaces or emerging from MMF under unstable environmental conditions without the need of any electronic stabilization system. The TWM involves the mixing of an object wave containing phase modulation and reference waves in a photorefractive crystal (PRC) where they create a light field known also as the interference pattern. The interference pattern is responsible for the recording of a dynamic hologram which is the periodical change of the refractive index. The hologram matches the wavefronts of the interfering waves and at the same time acts as an active filter which transforms in amplitude modulation only the fast phase changes while it rejects slow phase changes of the object wave. The linear transformation of the phase shifts relates with mechanism of hologram formation. In the drift mode of hologram formation, the linear regime of phase detection is achieved by applying an external dc-electric field to the crystal. Alternatively, the diffusion regime allows the less sensitive quadratic regime of the phase to intensity demodulation. However, also in the diffusion regime the linear detection of the phase shift can be achieved when the object and the reference wave have different polarization states. This last technique that we have mentioned is known as vectorial wave mixing (WVM).

In this thesis we present three novel configurations for multimode optical fiber sensor for the sensing of fiber strains induced by mechanical vibrations. Each sensor employs the VWM technique in a CdTe for the linear detection of multimode fiber strains. The first sensor that we present in

Papers II, III and **IV** is a one-channel sensor which is has been implemented by using the reflection geometry of hologram recording. The main features of principle of VWM in the reflection geometry of hologram recording are discussed in **Papers I, III** and **IV**. In **Paper II** we analyzed the performance of the sensor by using two fibers which have two different sizes of their cores. The second configuration of one-channel sensor which is introduced in **paper VI** uses VWM in the orthogonal geometry of hologram recording. In **Paper VI** and **VII**, we analyze the result of the holographic diffraction in the orthogonal geometry of wave mixing for CdTe. The third sensor, which we present in **Paper V**, is a multiplexed measuring system which employs several multimode optical fibers for the detection of mechanical vibrations. Each measuring channel of the sensor presented in **Paper V** is implemented by using the same scheme as it is shown in **Paper II, III** and **IV**.

Chapter 2

Photorefractive effect

The photorefractive effect is a nonlinear optical phenomenon which locally changes the refractive index of a photorefractive material which is illuminated by a spatially non-uniform light field [1-3]. To observe this effect, the material must possess both photoconductive and electro-optic properties. Materials which possess both these properties are called photorefractive. The photorefractive effect was first discovered in $LiNdO_3$, and it was considered to be an undesirable phenomenon because it was seen as a distortion of the transmitted light wave [4]. Nevertheless, since the discovery of such an effect many applications have been proposed. Photorefractive materials find potential applications in fields such as optical memory systems [5,6], optical information processing [7-9] and dynamic holography [10-12]. Materials which show photorefractive properties include ferroelectrics ($LiNbO_3$, $BaTiO_3$, $KNbO_3$,), sillenites ($Bi_{12}GeO_{20}$, $Bi_{12}TiO_{20}$, $Bi_{11}SiO_{20}$) and semiconductors (GaP, GaAs, InP,CdTe). The photorefractive effect is fundamental in the TWM technique because it is responsible for hologram formation. In this chapter we briefly explain how the wave coupling phenomenon gives rise to the formation of a hologram through the photorefractive effect.

2.1 Band transport Model

The most commonly used physical model, which describes the behavior of a photorefractive material, is the band transport model proposed by Kukhtarev *et al.* [13]. This model assumes that impurities contained in the material can be ionized under excitation of a light having a suitable wavelength, thus producing charges which can freely move in the material. More specifically, electrons from donor impurities are excited to the conduction band where they are free to move owing to the diffusion or the drift mechanism. The band transport model also assumes that all donor impurities have the same energetic levels, which are localized between the conduction and valence band as it is shown in figure (2.1). When the light does not have uniform distribution, the electrons generated in the brighter regions will obviously have higher concentrations than electrons generated in darker regions. Therefore, if no electric field is applied to the material, electrons generated in the brighter region will diffuse in the darker regions where they are recombined with other donor vacancies.

Let N_D be the concentration of donor impurities, N_D^+ be the density of ionized donors, n the concentration of free electrons in the conduction band, and I the optical intensity. If we neglect the

contribution of the thermal excitation, the rate of electrons generated in the conduction band is $sI(N_D - N_D^i)$, where s is the cross section.

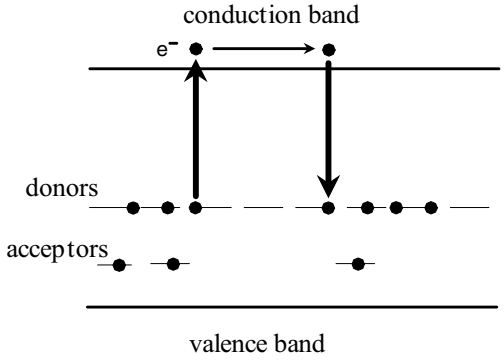

Fig. 2.1 Band transport model of the photorefractive effect

On the other hand, since electrons are re-trapped due to the concentration of the vacancies N_D^i, the recombination rate is $\gamma n N_D^i$, where γ is the recombination rate of the ionized vacancies. Therefore, the rate of ionized donors can be expressed by the equation

$$\frac{\partial N_D^i}{\partial t} = sI(N_D - N_D^i) - \gamma n N_D^i \tag{2.1}$$

and the rate of free electrons by the equation

$$\frac{\partial n}{\partial t} = \frac{\partial N_D^i}{\partial t} + \frac{1}{e}\frac{\partial j}{\partial x} \tag{2.2}$$

where t is the time, e is the charge of the electron, j the current density and x is the space. Equation (2.2) states that the concentration of free electrons is equal to that of ionized donors except for those electrons which are transported to the conduction band due to the current density j. When electrons migrate, there will be a change in the charge neutrality of the material. As a consequence, an electric field will appear. Such an electric field is termed the space charge field E^{SC}. When the space charge field appears, a drift current also appears. Such a drift current has the opposite direction to the diffusion current. Therefore, there will be a net electron current j which depends on both the diffusion of electrons in the material and the space charge field. The dependency is given as

$$j = k_B \mu T \frac{\partial n}{\partial x} + e\mu n E^{SC} \tag{2.3}$$

where k_B is the Boltzmann constant, μ is the mobility of charge carriers in the material and T is the absolute temperature. The Poisson equation provides the dependence between the electric field and the total charge

$$\frac{\partial E^{SC}}{\partial x} = \frac{e}{\varepsilon\varepsilon_0}(N_D^i - N_A - n) \tag{2.4}$$

where N_A is the concentration of the acceptor impurities and $\varepsilon\varepsilon_o$ the dielectric constant of the photorefractive media. The model developed by Kukhtarev *et al.* presumes that the acceptor impurities do not participate in the conduction and they are present in the material only in order to preserve the charge neutrality when the photorefractive material is not illuminated. Equations (2.3) and (2.4) describe the behavior of the photorefractive material when no external electric field E_0 is applied to the material. If an external electric field is applied to the crystal in the direction of the x-axis, then for both the equations we have to substitute E^{SC} with (E^{SC}+E_0). The equations shown above represent a simplified analytical model for analyzing the band transport model developed by Kukhtarev *et al*.

2.2 Space charge field

In this section we analyze the formation of the space charge field when two coherent light waves create an interference pattern in a sample of a photorefractive material (see figure 2.2). If the two light waves are represented by the vectors $\bar{A}$ and $\bar{B}$ with wave vectors $\bar{k}_A$ and $\bar{k}_B$ respectively. The spatial distribution of the intensity can be written as

$$I = I_0\left(1 + |m|\cos\left(\left|\bar{K}\right| \cdot x\right)\right) \tag{2.5}$$

where $I_0 = \left|\bar{A}\right|^2 + \left|\bar{B}\right|^2$ is the total intensity, $\left|\bar{K}\right| = \left|\bar{k}_A - \bar{k}_B\right| = 2\pi/\Lambda$, $\bar{K}$ is the grating vector, Λ is the grating period of the grating vector and m is the visibility defined by

$$m = \frac{2\bar{A} \cdot \bar{B}^*}{I_0} \tag{2.6}$$

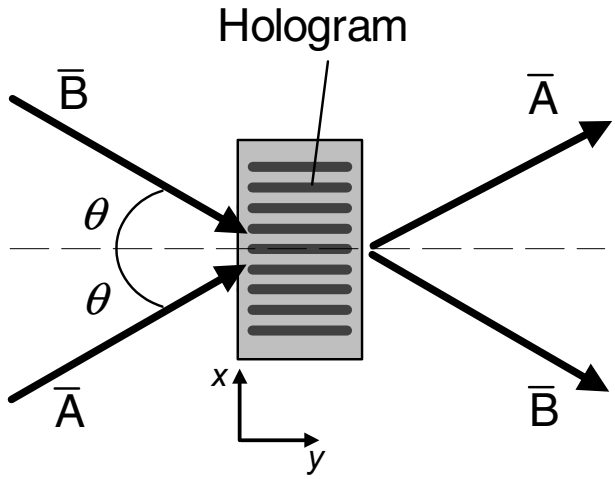

Fig. 2.2 Two-dimensional view of beams interaction inside the photorefractive crystal.

When the interference pattern arises, electrons are excited to the conduction band due to the absorption of photons in the bright regions. The electrons with energy in the conduction band are free to move, thus leaving behind donor impurities which remain positively charged. The charge redistribution gives rise to the space charge field which has distribution shifted by φ_0 in respect the interference pattern. The phase shift φ_0 is defined by the transport mechanism of the electrons in the conduction band during the process of formation of the space charge field. We will only consider the recording of the space charge field under stationary conditions. If during this process no external electric field is applied to the photorefractive material, the electrons move only due to diffusion mechanism. This last case is named to as the pure diffusion dominated regime of hologram recording [9,12,14,15].

Let us first estimate the amplitude of the space-charge field and the phase φ_0 for the pure diffusion dominated regime mechanism. The solution can be calculated from equations. (2.1)-(2.4) by assuming a small modulation index $|m| << 1$. This last assumption is verified in most experiments because the intensity of one of the two waves has usually smaller amplitude than the other wave $|B|^2 << |A|^2$. Let E^{SC} be the amplitude of the first harmonic of the space charge field. The equation which gives the solutions for the amplitude is given as [2]

$$\frac{\partial E^{SC}}{\partial t} + \frac{1}{\tau_M}\frac{E_M}{E_q}\frac{E^{SC}(E_q + E_d - iE_0)}{E_M + E_d - iE_0} = -\frac{m}{2}\frac{1}{\tau_M}\frac{E_M(E_0 + iE_d)}{E_M + E_d - iE_0} \qquad (2.7)$$

where τ_M is the Maxwell relaxation time, E_0 is the external electric field. The terms E_d, E_q, and E_M are the characteristic fields expressed as

$$E_d = \frac{KTk_b}{e} \qquad E_q = \frac{eN_t}{K}\varepsilon\varepsilon_0 \qquad E_M = \frac{1}{\mu\tau K} \tag{2.8}$$

where k_b is Boltzmann constant, N_t is the effective concentration of trap sites, μ is the mobility of electrons and τ is the life-time of electrons in the conduction band, E_d is the diffusion field which is proportional to the value of vector grating, E_q is the saturation field which is proportional to the trap sites and which defines the maximal amplitude of the space charge field that can be achieved in the crystal. The concentration of trap sites is equal to that of the donor acceptors, when the crystal is not illuminated. From equation (2.2) the solution for the steady state $\left(\frac{\partial E^{SC}}{\partial t} = 0\right)$ is given as

$$E^{SC} = -i\frac{m}{2}\frac{E_d E_q}{E_d + E_q} \tag{2.9}$$

The equation (2.9) shows that the amplitude of the space charge field is purely imaginary. Therefore, in the diffusion dominated regime there is a constant phase shift $\varphi_0 = \pi/2$ between the distribution of the space charge field and that one of the interference pattern. In contrast to the previous case, let us now consider case when an external dc-electric field is applied to the photorefractive crystal in the same direction of the vector grating. This case is named to as the drift dominated regime of hologram recording. Similarly as we have done in previous case, the solution for the steady state is now given by

$$E^{sc} = -\frac{m}{2}\frac{E_q(E_0 + iE_d)}{E_q + E_d - iE_0} \tag{2.10}$$

as one can see from equation (2.10) the amplitude of the space charge field is complex function of the applied field E_O. In most experiments it is usually verified the condition that $E_d << E_0 << E_q$. Therefore, the equation (2.10) takes the simpler form given by

$$E^{sc} = -\frac{m}{2}E_0 \tag{2.11}$$

The equation (2.11) shows that the space charge field is real. Therefore, when the electrons move

predominantly due to the drift mode the distribution of the space charge field is in phase or counter phase ($\varphi_o = 0,\pi$) with the distribution of the interference pattern. The last case that we analyze is the recording of the space charge field by applying an external alternating field with amplitude E_0 to the photorefractive crystal. This technique enhances the stationary grating of the space charge field by applying a square-wave alternating external electric field with period T to the photorefractive crystal [17-19]. Typically, the lifetime of the charge carriers (τ) is far shorter than response time (τ_R). If the condition $\tau << T << \tau_R$ is satisfied, we can assume that E^{SC} has a constant value ($\partial E^{sc}/\partial t = 0$) [17].

After averaging equation (2.7) over the period T and assuming that we have a small modulation index $m << 1$, in the steady state, amplitude of the first harmonic of the space charge field is given by [17]

$$E^{sc} = -i\frac{m}{2}\frac{E_O^2 E_q}{E_O^2 + E_q(E_d + E_M)} \tag{2.12}$$

The equation (2.12) shows that the amplitude of the space charge field is purely imaginary. Therefore, space charge field is $\pi/2$ phase shifted with respect the interference pattern like in case of the pure diffusion regime. However, as one can see from equation (2.12) the external electric field E_0 enhances the amplitude of the space charge field E^{SC} whereas the maximum value is the saturation field E_q.

2.3 Electrooptic effect

The space charge field in the photorefractive crystal modulates the refractive index of the crystal via the electro-optic effect. This causes a spatially varying refractive index grating to occur throughout the crystal. The pattern of the grating that is formed follows the light interference pattern originally imposed on the crystal by the interfering waves. In most cases of wave mixing in photorefractive crystals, we have the linear change of the refractive index (Pockel effect). The reason of that is that the space charge field is small compared with the internal field in the atom. As a result the quadratic and higher order effects are expected to be small compared with the linear effect. Moreover, the quadratic effect is usually neglected when the linear effect is present [20]. Note that such a condition is not valid for crystals which possess centro-symmetric structure. For those last crystals the quadratic effect is predominant. Therefore, the electro-optic behavior of the crystal which does not have centro-symmetric structure can be mathematically described by using the linear electro-optic tensor r_{ijk} [3,20]. This thesis focus the attention when recording of the space charge field is performed in a crystal of CdTe which belongs to cubic symmetry of $4\bar{3}m$. It is well known that the

symmetric properties of the tensor can reduce the complexity of its components because of the interchangeability of the first indices *i* and *j*. As consequence of these properties, the third order tensor r_{ijk} degenerates to a matrix of 6 x 3 elements, and some of these elements can be zero or identical depending on the point symmetry group to whom the crystal belongs. Therefore, the change of the tensor's permittivity ε_{ij} is given by

$$\Delta\varepsilon_{ij} = -n_0^4 r_{41} p_{ijk} \overline{E}_k^{SC} \tag{2.13}$$

where n_0 is the unperturbated refractive index, p_{ijk} is the normalized electrooptic tensor, and $\overline{E}_k^{SC}$ is the *k-th* component of the space charge field. In summary, the result of the mixing of two coherent light waves in a photorefractive crystal can be represented by five different processes: 1) photo-ionization of the donor impurities with consequent generation of free electrons having energy in the conduction band, 2) the free electrons migrate due to the diffusion or drift mechanism, 3) The electrons recombine with vacancies thus changing the charge distribution, 4) recording of the space charge field, and 5) recording of the index grating. After the electrons recombine with vacancies they can be re-excited and re-trapped, and so over and over again. Therefore, the index grating is a dynamic distribution continuously recorded in the photorefractive crystal.

2.4 Time of hologram recording

The time which occurs between the appearance of the interference pattern and the recording of the index grating is referred to as the response time of the photorefractive crystal. The response time of the photorefractive crystal is direct proportional to the Maxwell relaxation constant. The Maxwell relaxation constant is a measure for determining how fast the conducting medium reaches the electrostatic equilibrium [21]. Such measure takes into account the material properties and the average illumination intensity I_0 in the following manner

$$\tau_M = \frac{\varepsilon_0 h\nu}{e}\left(\frac{\varepsilon_r}{\tau\mu\alpha\beta}\right)\frac{1}{I_0} \tag{2.14}$$

where $h\nu$ is the energy of the absorbed light, α is the absorption coefficient of the photorefractive crystal, β is the quantum efficiency and the term in brackets represents the properties of the material. The coefficient of proportionality between the response time and Maxwell relaxation constant is defined by the transport mechanism of the free electrons. The response time is an important parameter which enables photorefractive material for adaptive interferometric purposes. This last aspect of photorefractive materials is discussed in section (3.3).

Chapter 3

Photorefractive wave-mixing

3.1 Coupled wave equations in scalar form

An interesting feature of the photorefractive effect is the possibility to manipulate the propagation of two light waves when they interfere in a photorefractive crystal. According to the theory described in chapter 2, the result of the wave mixing in a photorefractive crystal is the formation of the periodical index distribution, which is a replica of the interference pattern. The refractive index distribution diffracts both interfering waves because of the fulfillment of the Bragg condition [3,22]. Let us consider figure (2.2). The result of the diffraction is that wave *A* is scattered in the direction of wave *B* and vice verse, thus leading to the energy exchange between the two waves. Such a physical phenomenon is termed two-wave mixing (TWM) [23,24], whereas the index distribution is also termed a hologram. During diffraction from the hologram, the energy can flow from *A* to *B* or vice verse depending on the phase shift between the incident waves and the diffracted waves. The phenomenon of energy exchange during the diffraction from the hologram can be generally described by the scalar form of the system of coupled wave equations [3]. The scalar form of the coupled wave equations is a simplified mathematical model which treats the interfering beams as planar waves with scalar amplitude and which does not take into account their polarization properties. Nevertheless, it remains a very important mathematical tool for understanding the basic principle of energy exchange in TWM. Let us consider the case when the interfering waves propagate at a small angle θ along the *y*-direction as shown in figure (2.2). Let us also consider the same notation for optical wave amplitude used in section (2.2) but with the difference that now we are dealing with scalar quantities. The set of coupled wave equations in the scalar form is given by [3] as

$$\frac{dA}{dy} = -\frac{1}{2}\kappa\frac{B^2 A}{A^2 + B^2} - \frac{1}{2}\alpha A$$
$$\frac{dB}{dy} = \frac{1}{2}\kappa^*\frac{A^2 B}{A^2 + B^2} - \frac{1}{2}\alpha B \qquad (3.1)$$

where κ is a complex number representing the coupling constant which is given by

$$\kappa = i\frac{2\pi\Delta n}{\lambda\cos\theta}e^{-j\phi_0} \qquad (3.2)$$

where Δn is the amplitude of the modulated part of the refractive index, λ the wavelength and ϕ_0 is the phase shift between the space charge field and the interference pattern. Let us assume that the absorption of the material is negligible. Under this assumption, from the first equation of (3.1) we can deduce that the amplitude of A is an increasing function of the coordinate *y* provided by a negative value of the real part of the coupling constant. Note that the maximal value of Re $\{\kappa\}$ is obtained when the phase shift ϕ_0 between the space charge field and the interference pattern is $\pi/2$ radians. In this case we achieve the maximal energy transfer. The most fascinating application of the energy exchange in TWM is the demodulation of small phase shifts contained in one of the two interfering waves which are usually referred to as the object wave and the reference wave, the latter being unmodulated .

3.2 Coupled wave equations in vectorial form

Among the photorefractive materials, ferroelectrics ($LiNbO_3$, $BaTiO_3$) show the best light coupling properties. However, they do not possess the fast photorefractive response which is a necessary requirement for most industrial applications. Nowadays, much attention is being focused on cubic crystals such as sillenites (($Bi_{12}TO_{20}$ (BTO), $Bi_{12}SiO_{20}$ (BSO), $Bi_{12}GeO_{20}$ (BGO)) or semiconductors (CdTe, InP, GaAs), which are much faster than ferroelectrics, thus satisfying the necessary requirements for most practical applications. Unfortunately, the coupled wave equations in scalar form cannot fully describe the photorefractive wave mixing in crystals of cubic symmetry. One reason for this is that the result of the energy exchange in cubic crystals is highly sensitive to the polarization state of the input waves. Therefore, the energy exchange and the polarization states cannot be treated separately. Hence, the interfering waves must be treated as vectors describing both the amplitude and polarization state of the light field.

Several studies have been devoted to the vectorial nature of the energy exchange in photorefractive wave mixing [16,25-29]. Among these, the theory developed by Sturman *et al.*[16,30] is the most relevant because it describes almost all the phenomena of photorefractive mixing in cubic crystals. Such a theory underlines the importance of the polarization degree of freedom of the interfering waves and the orientation of the hologram with respect to the axes of the crystal in order to optimize the readout process.

The classical scheme of TWM is organized in the transmission geometry of hologram recording where the input waves enter the PRC from the same face of the crystal, thus co-propagating along the crystal at a small angle (see figure (3.1*a*)). Most studies on the photorefractive wave mixing have been focused on the transmission geometry of hologram recording. In this thesis we present the

results of the study of the photorefractive wave mixing field for different geometries of wave mixing.

In **Paper I** we present the results of the studies concerning the reflection geometry of wave mixing. In the reflection geometry of wave mixing, the input waves enter the crystal from opposite faces, thus counter-propagating inside the crystal, as shown in figure (3.1b). Let *s*,*p* be the unit vectors which define the directions of the polarization components of the input waves. Since we are considering the transverse nature of light propagation, we can define both the transmission and reflection geometry as collinear geometries due to the fact that polarization components of the interfering waves lie in the same plane, being perpendicular to the direction of propagation. In **Paper VI** we have shown the main advantages of the orthogonal geometry of wave mixing. In contrast to collinear geometries, in the orthogonal geometry the interfering waves enter the PRC from orthogonal faces, thus propagating in the PRC at ninety degrees to each other. In all our papers we restrict ourselves to the study of the pure diffusion regime of hologram recording in a CdTe cubic crystal which does not present optical activity. If A and B are Jones vectors describing the interfering waves, the set of coupled wave equations in vectorial form for all three geometries can be written as

$$\left(\frac{\partial}{\partial l_A}+\frac{\alpha}{2}\right)A(l_A)=-m\kappa\,\hat{H}\,B(l_B)$$

$$\left(\frac{\partial}{\partial l_B}+\frac{\alpha}{2}\right)B(l_B)=m\kappa^{*}\,\hat{H}\,A(l_A) \qquad (3.3)$$

where l_A and l_B are the directions of propagation of the waves A and B respectively, $m\kappa$ is the coupling constant, $\hat{H}$ is a dimensionless 2×2 matrix which depends on the relative orientation of the vector grating of the hologram in the photorefractive crystal. In **Paper I, III and IV** we compare the performances of the reflection with the transmission geometry of hologram recording. For the transmission geometry we have $l_A = l_B = x$ (see figure (3.1.a)), while for the reflection geometry we have $l_A = -l_B = x$ (see figure (1.b)), due to the fact that interfering wave counter-propagate. To observe efficient anisotropic diffraction from a reflection hologram, the grating vector should be oriented along one of the principal crystallographic axes of the crystal (the vector grating is oriented along the $[001]$-axis). Note that this condition is different for the transmission geometry, where the

anisotropic diffraction is most pronounced if the interfering waves propagate at a small angle with respect to the $[1\bar{1}0]$axis, in which case the grating vector is parallel to the $[110]$-axis. Since in the collinear geometry the waves travel in the same direction (see figure (3.1*a*)), the matrix $\hat{H}$ is the same for both waves and for the orientation of the vector grating 2:

$$\hat{H} = \begin{pmatrix} 0 & 1 \\ 1 & 0 \end{pmatrix} \tag{3.4}$$

Equation (3.4) states that the s-direction component (vertically polarized component) diffracts to the p-direction component (horizontally polarized component) and vice versa. In contrast to collinear geometries, the matrix $\hat{H}$ can differ for different waves in orthogonal geometry. At the same time, one can find a configuration where the coupling matrices for two waves are identical. For instance, it is fulfilled for the orthogonal geometry represented in figure (3.1c):

$$\hat{H} = \begin{pmatrix} 0 & \frac{1}{\sqrt{2}} \\ \frac{1}{\sqrt{2}} & 0 \end{pmatrix} \tag{3.5}$$

In **Paper I, III** and **IV** we show that the energy exchange of the interfering wave can be improved by using the reflection geometry of hologram recording. The coefficient κ in the presence of the pure diffusion regime of hologram recording can be expressed as

$$\kappa = \frac{\pi n_0^3 r_{41}}{\lambda} \frac{E_d}{1 + E_d / E_q} \tag{3.6}$$

Let us consider both equations (3.6) and the first equation of (2.8). From those equations we deduce that a simple way to increase the coupling coefficient is to increase the spatial frequency of the interference pattern by switching from the transmission to the reflection geometry of hologram recording. However, the increase of the coupling coefficient is achievable only for high values of the saturation field ($E_q >> E_D$). As shown in equation (2.8), the amplitude of the saturation field is directly proportional to the concentration of N_t. Therefore, by switching from transmission to orthogonal or reflection geometries, we are able to improve the coupling coefficient only if the PRC possesses quite high concentrations of photorefractive centers.

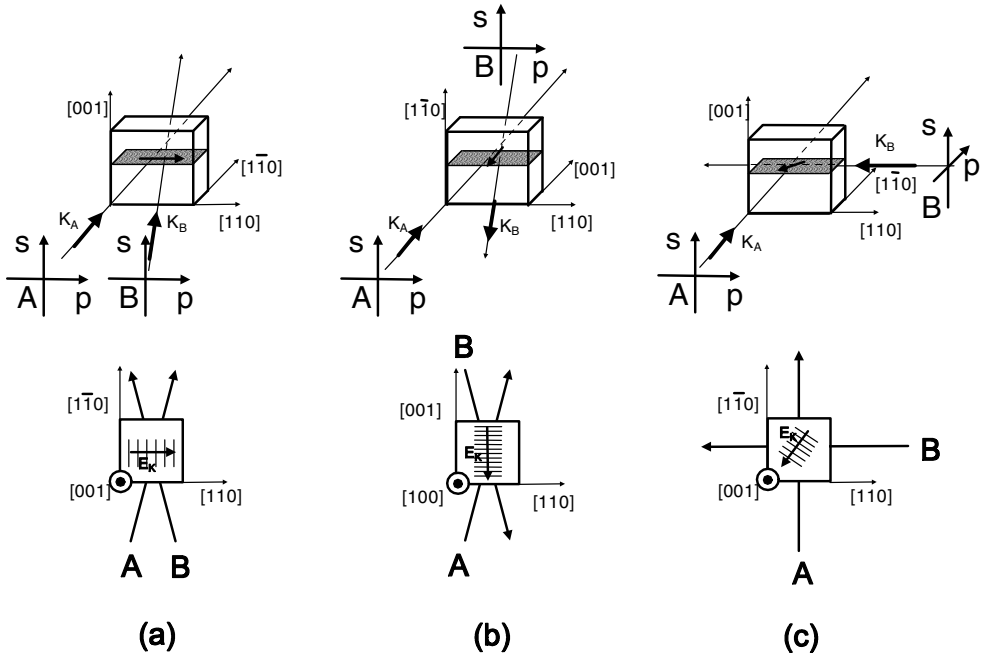

Fig. 3.1 Representation of the (a) transmission, (b) reflection and (c) orthogonal geometry when the orientation of the hologram allows anisotropic diffraction.

3.3 Self-adaptive holographic interferometers

Classical homodyne interferometers have two main limitations: they do not perform efficient phase demodulation when the object beam has a speckled wave front, and the instability of the working point when the interferometer operates in an unstable environment. There is no solution to the first limitation when conventional interferometers are employed. To stabilize the working point, the interferometer usually needs an electronic feedback system which makes the whole arrangement more complex [31,32].

The two-wave mixing technique represents a simple and elegant way for implementing self-adaptive interferometers [33,34]. These interferometers are also called self-adaptive holographic interferometers. The main difference between the classical homodyne interferometer and the self-adaptive holographic interferometer is that in the latter the beam splitter which combines the reference and object wave has been replaced with a hologram continuously recorded in a PRC (see figure (3.2)). One of the advantages of writing holograms in a PRC is the perfect reconstruction of light field wavefronts [35]. Owing to this principle, the wave front of the diffracted part of the

reference beam is the exact copy of the transmitted part of the object beam, and this also applies to the other couple of transmitted beams. Moreover, due to the dynamic nature of the hologram recorded in a photorefractive crystal, the wave fronts of transmitted beams are continuously matched even when one or both wavefronts of the input beams have a speckled time-varying distribution [36]. Another advantage of the dynamic hologram is its ability to preserve the phase difference of the matched waves in the steady state. When environmental parameters such as temperature or pressure affect one or both arms of the self-adaptive interferometer, a new phase difference appears between the input waves which enter the photorefractive crystal. Such phase difference shifts the distribution of the interference pattern. Therefore, as the new hologram is recorded within a time τ_R, the phase difference of the matched wavefront returns to its previous state. When we have periodical changes of the phase difference between the interfering beams with period T (i.e. the length of the measuring path is periodically modulated), there are two different behaviors of the crystal. If the period T is smaller than the response time τ_R of the crystal, the hologram cannot follows shifts of the interference pattern. Therefore, the moving interference pattern interacts with the frozen distribution of the hologram, thus permitting changes of intensity in the transmitted light. If the period T is larger than the response time τ_R, the hologram has time to be rerecorded and to follow the shifts of the interference pattern. Therefore, no intensity modulation takes place in the output beams. The properties mentioned above which are referred to as adaptability allow the elimination of low frequency noise caused by environmental parameters such as temperature or pressure.

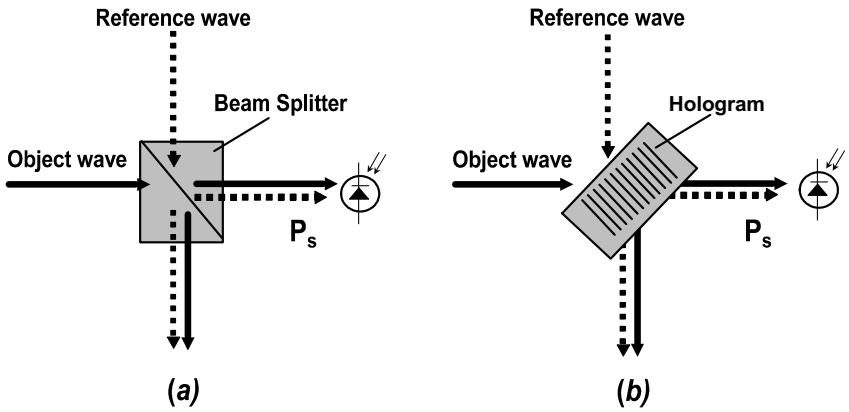

Fig. 3.2 Schemes of (a) classical homodyne interferometer and (b) self adaptive holographic interferometer.

3.4 Linear phase demodulation

The linear demodulation of small phase shifts encrypted in the object wave is a necessary requirement for any interferometer to achieve the highest sensitivity. This requirement is satisfied

when the phase difference between the non-diffracted object wave and diffracted reference wave is $\pm\pi/2$ radians (the quadrature condition). For a self adaptive holographic interferometer, the phase difference between the diffracted beams strongly depends on the mechanism of the hologram formation. As we have seen in section (3.2), for the drift mode of hologram recording the index grating distribution is in phase or counter-phase with the distribution of the interference pattern. Since the reference wave acquires an additional phase shift of $\pi/2$ radians after being diffracted from the hologram (Fresnel phase shift due to reflection), there will be a phase shift of $\pm\ \pi/2$ radians with respect to the transmitted object wave. Therefore, the hologram recorded in the drift dominate regime allows the direct fulfillment of the quadrature condition (i.e. when both waves have linear and parallel polarization state) [33]. However, applying a strong dc-external field has some disadvantages: the screening effect and the overheating of the photorefractive crystal's sample due to the strong dc-electric field which has typical amplitude of a few kV [37]. Therefore, such a technique may not be acceptable for many practical applications.

For the diffusion mode of hologram recording, the distribution of the hologram is $\pi/2$-phase shifted with respect to the interference pattern as shown in equation (2.9). Therefore, after diffraction there will be a 0 or π-phase shift between the diffracted reference wave and the transmitted object wave. Therefore, the hologram recorded in the diffusion regime does not directly support the linear phase demodulation.

Many schemes of two wave mixing have been proposed to achieve the linear phase demodulation in the diffusion mode [14,38-39]. For all those cases the linear regime of the phase demodulation is achieved either by installation of a polarizer or a polarization beam-splitter before the photo-detector. Unfortunately, the presence of a polarizer filtering before the photodetector introduces optical losses, leading to worsening of the sensitivity of the interferometer. In reference [40] it is shown that the linear phase demodulation can be achieved in the diffusion mode of hologram recording and in the geometry of anisotropic diffraction when the object and reference wave have linear and elliptically polarization states, respectively. In contrast to previous proposals [14,38-39], in the scheme of photorefractive wave mixing presented in reference [40] no polarizing element is placed before the photodetector.

When light diffraction has an anisotropic character (diffraction is accompanied by rotation of the polarization state of ninety degree), we can achieve the quadrature conditions even in the diffusion mode of hologram recording because the inherent $\pi/2$ phase difference between the orthogonal components of the (x and y) of the elliptically polarized wave is transferred into an interference term of the transmitted and the diffracted wave. The technique which is presented in reference [40] is termed vectorial wave mixing (VWM). In **Papers I-VI** we have employed the VWM for the linear demodulation of phase shifts contained in the light wave emerging from a MMF. Since in those configurations a linearly polarized object wave is required for the achievement of the quadrature

condition, a polarizing element has to be installed at the fiber's output. Unfortunately, as we have shown in **Paper II,** the presence of the polarizer leads to the appearance of polarization noise. In section (4.2) there is a detailed discussion of the polarization noise and how to diminish its level.

In contrast to the collinear geometry of wave mixing, in **Paper VI** we show that the orthogonal geometry of wave mixing allows linear phase demodulation even when phase transients are encrypted in a depolarized wave without using any polarizing element. Using the vectorial wave coupling theory [16], the analytic solutions for the output intensities of the interfering waves can be obtained in the presence of fast phase modulation in one of the interfering waves.

In **Paper VII** we have analyzed and compared different geometries of wave mixing by using a common approach which studies the intensity of the object transmitted through the PRC with a thickness L. In our analysis we considered the undepleted pump approximation. Moreover, we also considered that both the amplitude of the reference wave and the half-contrast *m* do not depend on the direction of propagation. Let us consider again the Jones vectors of the waves A and B. From the first equation (3.3) we can estimate the amplitude of the object wave at the crystal output:

$$A' = A + \Delta A = A - L_A m \kappa \hat{H} \cdot B \tag{3.7}$$

where ΔA is the change of the intensity of the object wave at the crystal's output, L_A is the crystal's length along the direction of propagation l_A. Now let us consider the interaction of two waves in collinear and orthogonal geometries. Taking into account the transverse nature of an electromagnetic wave, we represent their amplitudes by Jones vectors having two polarization components: one of them (*s*) is orthogonal to the plane formed by wave vectors k_A and k_B, while the other (*p*) belongs to the plane (k_A, k_B). Let us first consider the case when the object wave and the reference waves are linearly and elliptically polarized, respectively. The wave amplitudes can be represented as

$$A = \begin{pmatrix} a_s \\ a_p \exp i\alpha \end{pmatrix} \qquad B = \begin{pmatrix} b_s \\ b_p \exp i\delta \end{pmatrix} \tag{3.8}$$

Where α and δ are phase differences between orthogonal components of the object and reference waves, respectively. In the collinear geometry of wave mixing the vectors A and B lie in the same plane (see fig. (4.1.*a,b*)). Therefore, the half-contrast can be written as

$$m = \left\{ a_s b_s + a_p b_p \exp[i(\alpha - \delta)] \right\} I_0^{-1} \tag{3.9}$$

As one can deduce from equation (3.9), the hologram recorded in the collinear geometry can be considered to be the superposition of two mutually orthogonal gratings shifted by a phase $\alpha - \delta$. Each polarization component of the interfering waves can diffract from both of these gratings, producing an interference signal. Now, let us suppose that we introduce in the object wave a fast phase transient with a transient time shorter than recording time of the hologram. This situation is analytically described by just multiplying the vector A by a phase factor $\exp(i\phi)$ in equations (3.8) while *m* is kept constant. After the mixing of the object wave with the elliptically polarized reference wave in collinear geometry, the intensity of the of the phase-modulated object wave mixed with the reference wave in the photorefractive crystal wave is given by

$$I'_A = I_A + 2|\gamma|^2 I_B + \Delta I(\phi) \tag{3.10}$$

where $\gamma = \gamma_s + \gamma_p \exp(i\delta)$, $\gamma_s = \frac{\kappa L_A}{I_0} a_s b_s$, $\gamma_p = \frac{\kappa L_A}{I_0} a_p b_p$ and $\Delta I(\phi)$ is the intensity change caused by phase modulation of the object wave, which is given by

$$\Delta I(\phi) = -2[a_s b_p \gamma_s \cos(\phi - \delta) + a_s b_p \gamma_p \cos(\phi - \alpha) + a_p b_s \gamma_s \cos(\phi + \alpha) + a_p b_s \gamma_p \cos(\phi + \delta)] \tag{3.11}$$

As one can see from equation (3.11), the interference signal $\Delta I(\phi)$has four components. Each component of the interference signal $\Delta I(\phi)$ is the product of a diffracted component of reference wave and a transmitted component of the signal wave. It is clear from equation (3.11) that if both input waves have the same linear polarization state (i.e., if α= 0 and δ = 0), we have only the quadratic regime of phase demodulation $\Delta I(\phi) \sim (1 - \phi^2/2)$, for $\varphi << 1$. In contrast to this last condition, if the reference wave is elliptically polarized ($\delta = \pi/2$), from equation (3.11) we obtain

$$\Delta I(\phi) \approx -2\kappa L_A I_0^{-1}\left[b_s b_p (a_s^2 - a_p^2)\phi + \sin\alpha \cdot a_s a_p (b_s^2 - b_p^2)\phi + \cos\alpha \cdot a_s a_p (b_s^2 + b_p^2)(1 - \phi^2/2)\right] \tag{3.12}$$

As one can see from first term of equation (3.12), the first two terms between square brackets are both proportional to ϕ. Therefore, the collinear geometry provides linear phase demodulation.

When the object wave is depolarized, we can characterize it by two mutually orthogonally and independent polarization components with almost equal intensity ($a_s \approx a_p$). Consequently, the first term in equation (3.12) becomes zero. Therefore, if the reference wave has circular polarization state ($b_s = b_p$), we have again only a quadratic regime. It is worth noting that the linear phase demodulation disappears as well if the signal wave is linearly polarized but at 45 degrees to the *s*- (or *p*-) direction ($a_s = a_p$ and $\alpha = 0$). Thus, in collinear geometry, the linear demodulation of phase is

possible if the signal wave has only an *s* or *p* polarization component, or one of these components prevails.

In the orthogonal geometry of wave mixing, only the *s*-polarization components of the input waves interfere and record the hologram because the *p*-components are mutually orthogonal. Therefore, only one term appears in equation (3.9):

$$m = a_s b_s I_0^{-1} \tag{3.13}$$

If we mix a linearly polarized object wave and elliptically polarized reference in the orthogonal geometry of wave mixing, the intensity of the object wave at the crystal's output can be expressed as

$$I'_A = I_A + \frac{\gamma_s^2}{2} I_B + \Delta I(\phi) \tag{3.14}$$

If we consider again the case of an elliptically polarized reference wave where $\delta = \pi/2$ and $\phi << 1$, we can calculate the change in the intensity of the signal wave thus:

$$\Delta I(\phi) = -\sqrt{2}\gamma_s \left[a_s b_p \phi - \sin\alpha \cdot a_p b_s \phi + \cos\alpha \cdot a_p b_s (1 - \phi^2/2) \right] \tag{3.15}$$

As one can see from equation (3.15), the first term, which is responsible for linear phase-to-intensity transformation, is nonzero for any polarization state of the object wave except when this wave is linearly polarized along the *p*-direction (i.e. when a_s = 0). Therefore, in contrast to collinear geometries, in the orthogonal geometry we can achieve linear phase demodulation for any orientation of linearly polarized object waves except the case when the linear polarization state is oriented along the *p*-direction (i.e. when a_s=0). It is worth nothing that when a_s=0 in the orthogonal geometry, no hologram will be recorded. Consequently, in this case we will not have even a quadratic regime of phase demodulation. In all other cases we have a linear regime of phase-to-intensity transformation. Therefore, we can conclude that orthogonal geometry of wave mixing provides the linear phase demodulation even for depolarized object waves.

3.5 Sensitivity

A desired requirement for any interferometer is the ability to detect the smallest phase shifts which encode the physical parameter to be measured. Qualitatively, the performance of any interferometer can be estimated by comparing its sensitivity with that of the classical lossless interferometer

[41,42]. The minimal detectable phase shift is defined by the biggest source of noise present in the measuring system. There are several sources of noise which can limit the sensitivity of the interferometer [43,44]. However, when the intensity of the light beam which reaches the photodetector is quite high, the shot noise becomes predominant over all the other sources of noise. The shot noise in optical devices is related to the quantum nature of light. When light reaches the photodetector, the shot noise manifests itself through instabilities in the electric current caused by statistical fluctuations of the photons. Therefore, such a noise depends on the average intensity of the light beam which reaches the photodetector. The dependence is given as

$$\left\langle i_{shot}^2 \right\rangle = 2\frac{e^2\eta}{h\nu}\left\langle P_D \right\rangle \Delta f \tag{3.16}$$

where η is the quantum efficiency, P_D is the intensity of light which reaches the photodetector, and Δf is the frequency bandwidth of the measuring electronic system. Now let us consider the classical interferometer as shown in figure (3.2.a). Let us suppose that we introduce a small phase shift ($\phi << 1$) in one of the input waves. The intensity of the light which reaches the photodetector is the sum of the non-modulated part P_S and of the modulated part ΔP_S. The modulated part ΔP_S contains the linear modulation which encodes the informative signal proportional of the physical parameter to be measured. The non-modulated part P_S is responsible for the shot noise. The general form of the signal-to-noise ratio is given by [44] as

$$SNR = \frac{\Delta P_S}{Q\sqrt{P_S}} \tag{3.17}$$

where $Q = \sqrt{4\Delta f h\nu/\eta}$. The minimal detectable phase shift can be theoretically calculated by equalizing the *SNR* to the unit. If the power of the reference wave is much bigger than power of the object wave $P_0^{'}$, we can assume that $P_S = 2P_0^{'}$ and $\Delta P_S = 2P_0^{'}\phi$. Therefore, the minimal detectable phase shift for the classical lossless interferometer adjusted to the quadrature condition with is given as

$$\phi_C^{\lim} = \frac{Q}{\sqrt{2P_0^{'}}} = \sqrt{\frac{2h\nu\Delta f}{\eta P_0^{'}}} \tag{3.18}$$

Let us now consider the minimal detectable phase shift $\Delta\phi_A^{\lim}$ of the interferometer under analysis. In our case the interferometer under analysis is the self-adaptive holographic interferometer (see figure (3.2.b).The theoretical estimation of $\Delta\phi_A^{\lim}$ should be carried out by considering the same

power of the object and reference waves entering the crystal, the same photodetector, and the same electronic measuring system as for the classical homodyne interferometer. It is obvious that the result of this estimation depends on many factors such as the particular setup which has been used to implement the interferometer, the coupling coefficient and absorption of the crystal. Once we find the proper expression of $\Delta\phi_A^{\lim}$, we can describe the performance of the interferometer under study by introducing the parameter

$$\delta_{rel} = \frac{\phi_A^{\lim}}{\phi_C^{\lim}} = \frac{SNR_C}{SNR_A} \tag{3.19}$$

Equation (3.19) is referred to as the relative detection limit of the interferometer under study. Since the SNR_C in the classical lossless interferometer is theoretically the highest achievable, the ratio in equation (3.19) is always bigger than 1. Therefore, the smaller its value, the more sensitive is the interferometer to the smallest phase shifts. It is clear that equation (3.20) provides only a theoretical estimation of the sensitivity.

Let us now see how to measure the detection limit in experiments. When a phase shift is introduced in the object beam, the photodetector will measure a variation of the intensity of the object beam ΔP_S whereas the nonmodulated part of the object beam will be $P_S = T_t P_0^{'}$, where T_t is the transmission coefficient which takes into account losses in the photorefractive crystal, and $P_0^{'}$ is the intensity of the object beam before the crystal. If we substitute P_S in equation (3.18) we obtain

$$SNR_A = \frac{1}{Q}\frac{\Delta P_S}{\sqrt{T_t P_0^{'}}} \tag{3.20}$$

Equation (3.20) gives the experimental measure of SNR_A. At this point, the experimental value of the relative detection limit can be calculated by substituting equations (3.18) (calculated for the lossless interferometer) and (3.20) in equation (3.19). The result is given by

$$\delta_{rel} = \sqrt{\frac{2}{T_t}}\frac{P_S}{\Delta P_S}\phi \tag{3.21}$$

The detection limit of a self-adaptive holographic interferometer depends on the light coupling efficiency. The higher the latter, the higher is the sensitivity to small phase excursions. Semiconductor materials such as GaAs, CdTe, and InP do not have efficient light coupling. Therefore, in these materials the light coupling must usually be enhanced by applying a strong ac-

field to the crystal. In **Paper I** we show that the efficiency of the holographic diffraction in CdTe can be further improved by switching from the transmission to the reflection geometry of the hologram recording. As a result, we will increase the detection limit of the interferometer to the smallest phase excursions. In **Paper I** we have experimentally measured the detection limit of the self-adaptive holographic interferometer as a function of the holographic grating period Λ, which determines the coupling constant in accordance with equation (3.6). Moreover, we compared the measurements of δ_{rel} for the transmission and the reflection geometry for two different samples of CdTe photorefractive crystals. The samples of CdTe were distinguished by the abbreviations BR-4Z-05 and BL-07-B1. The experimental graphs of figure (3.3) show the decreasing of δ_{rel} for both samples of CdTe, when Λ decreases. However, after switching from the transmission to the reflection geometry the decrease is more pronounced for sample BR-4Z-05 than for BL-07-B1. Such a difference appears because of the higher concentration of photorefractive centers (N_t) in BR-4Z-05. Similar results are also shown in **Papers III and IV**.

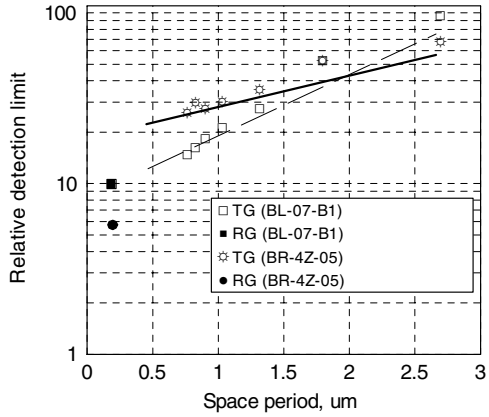

Fig. 3.3 Relative detection limits of the interferometer as a function of the grating period. Circles relate to sample BR-4Z-05, squares to sample BL-07-B1; filled shapes are for reflection geometry, open shapes for transmission geometry.

3.6 Photorefractive response

Due to the inertia of the hologram recording, a self-adaptive holographic interferometer can be described by the same typical transfer function used for a high pass RC filter [45]. Therefore, we can characterize the holographic interferometer by using the lower cutoff frequency

$$f_{cut} = \frac{1}{2\pi\tau_R} \tag{3.22}$$

As we have pointed out in section (2.4), the time constant τ_R is proportional to the Maxwell relaxation time. If we substitute equation (2.14) in equation (3.22), we get the following expression:

$$f_{cut} \approx \frac{e}{2\pi\varepsilon\varepsilon_0}\frac{\alpha\mu\tau\beta}{h\nu} I_0 \tag{3.23}$$

Equation (3.23) shows that fast materials should have a high mobility-lifetime product and/or high absorption. Moreover, the cutoff frequency can be enhanced by increasing the total light intensity I_0. In industrial applications, it is very often required to achieve a high rejection rate of noise at 50/60 Hz. Consequently, the response time should be faster than 300 μs, which corresponds to the low cutoff frequency of 500 Hz.

In **Paper I** we have experimentally investigated the dependency of the cutoff frequency as a function of the averaged intensity I_0 for both samples of CdTe. When the total average intensity was 40 W/cm^2, we have measured a cutoff frequency of 300 Hz for BR-4Z-05 and 1250 Hz for BL-07-B1. The sample BR-4Z-05 has a smaller cutoff frequency because of the larger concentration of photorefractive centers. These last results show the trade-off between detection limit and cutoff frequency in the interferometer. When the interferometer uses a faster crystal, it gains a higher rejection rate to slow noisy phase shifts. However, such a gain involves a sacrifice in terms of detection limit, as was shown in the previous section.

Chapter 4

Self-adaptive fiber-optic sensors

During the past thirty years, the growth of fiber-optic communications and optoelectronic industries has contributed hugely to the development and commercialization of many types of optical fiber sensors. Nowadays, fiber sensor systems have benefited the most from such technologies [46-48]. The main advantages of fiber sensors are compactness, lightweightness, robustness, passiveness, immunity to electromagnetic interference, and high sensitivity. Compared with conventional transducers, optic-fiber sensors perform quite well and in principle are cost effective. However, the new technology for the production of optic-fiber sensors is usually more costly than the well-established technology for producing conventional transducers. Consequently, fiber sensors are particularly used in applications with special requirements, such as non-electrically active sensor heads, extremely light devices, and efficient multiplexed sensor systems. In their simplest implementation, optical fibers may be used only to convey the optical signal to and from the headset of the optical sensor. Nevertheless, optical fibers can also be used as sensors for the detection of various physical parameters such as temperature, pressure or mechanical stresses [49,50].These physical parameters change the properties of light such as intensity, phase, polarization state and frequency. The main advantage of a fiber-optic sensor is the ability to detect these changes with high sensitivity.

4.1 Sensing of multimode optical fiber strains

One of the mechanisms of optical-fiber sensing is to convert the fiber strains caused by external parameters into changes of the phase ($\Delta\phi$) of the light traveling inside the optical fiber. Hence, interferometric measuring systems should be employed to detect phase changes with high sensitivity. Conventional interferometers require two interacting waves with identical polarization state to ensure highly fringes visibility. Such a requirement is easily achievable when, for instance, the sensitive arm of the interferometer is a single mode fiber (i.e. polarization-maintaining optical fiber). However, in some practical cases using a multimode optical fiber (MMF) is much more convenient than using a single mode fiber.

Compared with a single mode fiber, the multimode type possesses higher numerical aperture and higher light power carrying capacity. Moreover, multimode optical fibers allow the easier implementation of efficient multiplexed fiber sensors. However, as we have outlined in section (3.3), during operative conditions conventional interferometer do not perform well with MMF. Since a MMF has a bigger core than a single mode fiber, the light propagation in a MMF is characterized by more than one propagation mode. When highly coherent light travels through the MMF, the

resulting wave at the fiber's output is characterized by a random distribution of the intensity and polarization state of the light due to the intermodal interference. Whenever external parameters such as temperature, pressure or even mechanical vibrations affect the MMF, they also affect the propagations of spatial modes in MMF, thus changing the distribution of the light field at its output. T. Hall *et al.* [36] were the first to propose the use of photorefractive wave mixing in PRC as a technique to implement self-adaptive interferometers for efficient demodulation of phase shifts encoded in a depolarized object wave emerging from MMF. Later, other proposals [51,52] have confirmed that photorefractive wave mixing is one of the most efficient techniques for compensating for instabilities of wavefront such as those emanating from MMF.

In **Paper II** we have reported on the performance of a sensor configuration for efficient detection of MMF strains induced by mechanical vibrations. The sensor configuration has been implemented by using the VWM in the reflection geometry of hologram recording in CdTe photorefractive crystal. In contrast to previous proposals [36,51,52], the great advantage of our configuration is that the VWM in the reflection geometry in CdTe allows the linear detection of phase shift without applying any external field to PRC. The scheme of the sensor is schematically shown in figure (4.1). In the configuration, the object and the reference waves are both originated from a light beam which has high coherence length (100 m) and which is generated by a CW Nd:YAG laser (λ = 1064).

In experiments, the MMF was tightly reeled onto a piezoelectric ring which was electrically driven by a sinusoidal voltage with frequency *f,* thus modulating the phase of the light at the same frequency. The polarization states of the waves which enter the PRC are elliptical and linear for the reference and object wave, respectively. To this end, a polarizer has to be installed to select the linear polarization state from the depolarized wave emerging from the MMF, whereas the polarization state of the reference wave is controlled by an adjustable wave plate. After the polarization filtering, the waves are launched in the PRC (CdTe), where they propagate along the <001> crystallographic axis. As was mentioned in section (3.2), this arrangement of the wave mixing allows efficient holographic diffraction in the reflection geometry of hologram recording without applying any external field to the PRC. A conventional photodiode is placed after the crystal to measure the intensity of the transmitted wave. Owing to the principle of VWM, the phase modulation of the object wave emerging from the MMF is linearly transferred in intensity modulation of the transmitted wave after holographic diffraction. Consequently, the signal detected by the photodiode is modulated at the same frequency as the excited dynamic strains. When voltage is applied to the piezoelectric cylinder, we modulate a small displacement of the outer surface.

The ability of the sensor to measure such small displacements depends on many factors. One is the ability of the MMF to transform mechanical vibrations into phase shift of light traveling through the fiber. Another is the interferometer's ability to detect the smallest phase shift caused by fiber strains. As we have seen in section (3.5), this last factor depends on the noise level of the measuring system.

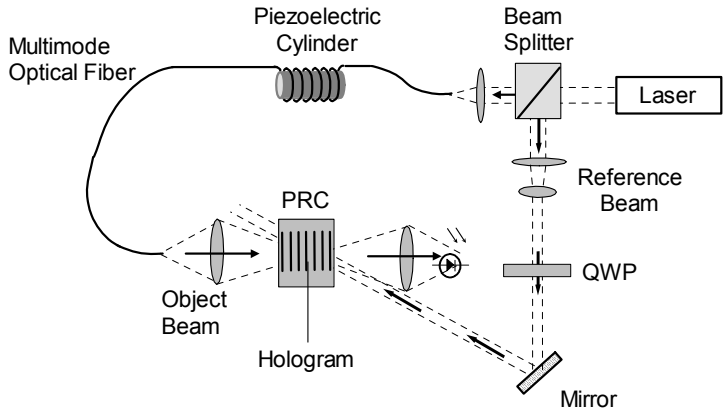

Fig. (4.1) Optical scheme of the multimode-fiber strain sensor stabilized via vectorial wave mixing in a photorefractive CdTe crystal operating in the reflection mode.

4.2 Polarization noise

In **Paper II** the performance of the optic fiber sensor was studied for two different fibers with different core diameters, 50 μm and 560 μm. Such fibers are typically used in optic communications. During the sensitivity study, it was observed that the biggest source of noise was related to the instabilities in the distribution of the light emerging from the MMF. This noise appeared when a polarizer was placed in front of the output of the MMF, and it manifested itself through the appearance of instabilities in the amplitude of the signal detected by the photodiode during the phase demodulation. These instabilities were much slower (tens of seconds) than the response time of our fast crystal in spite of the fact that slow phase changes of the speckle pattern are expected to be compensated for by the dynamic hologram.

The noise could be isolated by blocking the reference wave. In this case, the signal detected by the photodiode appeared at the same frequency f but with smaller amplitude. This amplitude was unstable with a stochastic appearance of $2f$-modulation and sometimes with the opposite sign. Note that this kind of modulation is typically observed when a light beam emerging from the MMF strikes any spatial aperture before being captured by a photodiode. In our experiment, all the light emerging from the fiber was completely collected into the active area of the photodiode so that no modulation was observed without a polarizer and reference wave. Though this unstable signal was modulated at the excitation frequency f, we classified it as a "polarization" noise because it leads to uncertainty in phase excursions measurement.

The origin of this noise is the stochastic distribution of the polarization state among different speckles at the output of the MMF. When we install the polarizer which is needed in the configuration of VWM, we select the main component of the set of all speckles of the wavefront.

Any external impact on the fiber (such as temperature, pressure, or bending, including periodically introduced strains) affects the mode propagation, thus changing the size and polarization state of each individual speckle. Consequently, there will be a change of the amplitude and polarization state of the main component. In this way, periodically modulated strains of any multimode fiber produce not only phase modulation but also intensity modulation at the frequency of *f*. At the same time, since the orientation of the main polarization component slowly changes due to slower environmental parameters such as temperature or pressure, we can also observe the appearance of the second harmonic at *2f*.

In **Paper II** we have reported on the experimental measurement of the polarization noise for both fibers. We have found that the noise level in the thick fiber was one order of value smaller than in the case of thin fiber. As we have already mentioned, the amplitude of the polarization noise is related to the statistical distribution of the finite number of speckles at the fiber output. The larger the core of the fiber, the higher the number of spatial modes travelling into the fiber, and consequently also the higher the number of speckles at the fiber's output. Therefore, the higher the number of speckles, the smaller the probability that all speckles will have a polarization state oriented in the same direction.

The fiber with a thin core can support 420 spatial modes at a wavelength of 1064 nm. In contrast to the thin fiber, the thick fiber can support 53,000 spatial modes at the same wavelength. Therefore, we deduce that when the fiber with a thick core is employed, the amplitude of the main component should be smaller, resulting in a decrease of the polarization noise. The diminishing of the polarization noise enables the interferometer to measure the smaller phase shifts. Figure (4.2) shows the dependence of the signal-to-noise ratio (SNR) on the amplitude of phase modulation at $f = 1$ kHz and $f = 10$ kHz for both fibers.

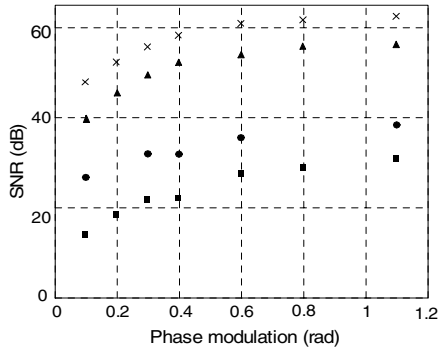

Fig. 4.2 Signal-to-noise ratio as a function of the phase-modulation amplitude in 50-μm-core fiber at 1 kHz (squares), at 10 kHz (circles), and in 550-μm-core fiber at 1 kHz (triangles), and at 10 kHz (crosses).

As can be seen from figure (4.2), the signal to noise ratio is bigger for the fiber with a thick core due to the smaller amplitude of the polarization noise. The minimal detectable strain in the thin fiber ($8.5 \cdot 10^{-5}$ με) was higher than that for the thick fiber ($1.5 \cdot 10^{-5}$ με). However, when the amplitude of phase modulation was bigger than the minimal detectable phase shift, the sensitivity of both fibers was the same (0.083±0.008 radians/με per centimeter).

In **Paper VI** we have proposed the orthogonal geometry of wave mixing sensor for the detection of strains of the MMF. The sensor is schematically shown in fig. (4.3). As we have seen in section (3.4), the most important advantage of the proposed geometry of waves mixing in PRC is its ability to provide linear demodulation of small transient phase changes encrypted even from object depolarized waves without any polarizing element and without applying any external electric field to PRC. The performance of the orthogonal geometry of wave mixing was studied when phase shifts emerge from the fiber having a thick core.

The experimental setup was similar to that one used in **Paper II,** whereas the vector grating of the hologram recorded in the orthogonal geometry is oriented along the crystallographic axis [010], as it is shown in Fig. (3.1c). The performance of the sensor was studied for the both cases when no polarizer was installed and when polarizer was installed in front the output of the MMF. Like in experiment described in **Paper II**, all the light emerging from the fiber was completely focused in the active area of the photodiode. We found that the level of the polarization noise was one order of value smaller when polarizer was not installed. The presence of residual noise probably related with factors such as the imperfections of the crystal or no perfect polishing of the MMF´s output. Such factors may cause scattering of the light emerging from MMF. Consequently, the light emerging from the fiber cannot be completely collected into the photoreceiver.

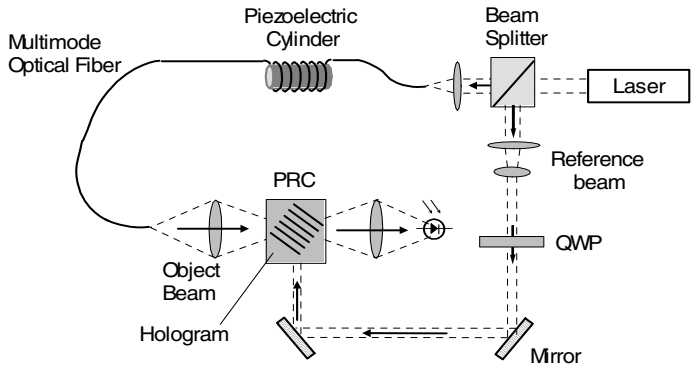

Fig. 4.3 Optical scheme of the multimode-fiber strain sensor for linear detection of phase shifts from depolarized object wave operating in the orthogonal geometry of wave mixing.

4.3 Multiplexing

In many practical situations (e.g. vibration monitoring in industrial environments), it is desired to use a multiplexing sensor in order to address many transducers situated in different points of the area under study. Some important requirements for multiplexing sensor are: the possibility to implement a large number of measuring channels, high sensitivity for each measuring channel, the compensation of environmental instabilities and the low crosstalk. Due to these requirements the implementation of multiplexing sensor can be a very tough task.

The TWM technique is very advantageous technique because it offers the possibility for easy multiplexing of different self-adaptive interferometers using a single PRC. This variant of photorefractive wave mixing has been named to as multi two-wave mixing (MTWM). In MTWM a single reference wave is coupled in a single PRC with several object waves which emerge from the different measuring channels. This approach of sensor multiplexing allows the simultaneous phase detection from all measuring channels. A survey on scientific literature reveals that MTWM has been employed for multiplexing of sensors for detection of mechanical vibrations [53-55]. In those configurations, the wave coupling was implemented by using the transmission geometry of wave mixing whereas the object and reference waves enter the PRC from the same face of the crystal. Each object records a hologram with the reference for demodulation of the phase shifts of the wave emerging from its respective measuring channel. However, since the object-to-object interference records secondary holograms, such holograms couple the object waves thus leading to crosstalk

between different measuring channels. Moreover, since all the object waves interfere with a single reference, it is usually necessary to focus them in the same portion of crystal. By this way, it is obvious that the higher the number of measuring channels the higher the crosstalk. Therefore, the maximum number of measuring channels is defined by the maximal crosstalk level that we can accept. Moreover, as reported in references [53-55] the linear phase demodulation was supported by applying a strong electric external field to the PRC.

In **Paper V** we present a configuration of multiplexed fiber optic sensor for detection of mechanical vibrations. The sensor uses a novel geometry of multi wave coupling based on the VWM in the reflection geometry of hologram recording in single photorefractive crystal of CdTe without applying any extermal electric field. In **Paper V** the implementation of each measuring channel is done exactly in the same way as shown in **Paper II**. The figure (4.4) shows case when the sensor incorporates only two measuring channels.

The most important feature of the multiplexing sensor presented in **Paper V** is the very low crosstalk between the measuring channels. In configuration, the object waves emerging from MMF enter the PRC from the same face of the sample while the reference wave enters the crystal from the opposite face. The reference wave is elliptically polarized while the object waves have the same linear polarization states. The linear polarization state for all object waves emerging from MMFs can be selected by positioning a single polarizer before the PRC. All the waves travel in the crystal at small angle along the crystallographic axis [001]. Therefore, the reference and each object waves record a hologram with vector grating oriented to the axis [001]. As we have mentioned in section (3.2), this last condition is optimal to achieve efficient holographic diffraction in the reflection geometry, thus allowing efficient phase demodulation from each measuring channel. The object-to-object wave pairs also record holograms of the transmission type in our geometry of wave mixing. However, since such secondary holograms has vector grating also perpendicular to the axis [001], they do not couple the object waves. The reason why is because of the specific feature of the electro-optic tensor of cubic crystals like CdTe. The transverse electric field does not change the propagation constant of the light wave when it propagates along one of the principal axis [20]. Therefore, our configuration should not allow crosstalk between different measuring channels.

Another advantage of our sensor is that the reflection geometry possesses a higher angle-degree of freedom than transmission geometry. In the reflection geometry, the angle of incidence of the object beams may vary arbitrarily in two dimensions without dramatically changing the orientation of reflection holograms. In contrast, only one plane of incidence for all object beams is allowed in the transmission geometry. For more clearness the geometry of multiple wave interaction is shown in figure (4.5).

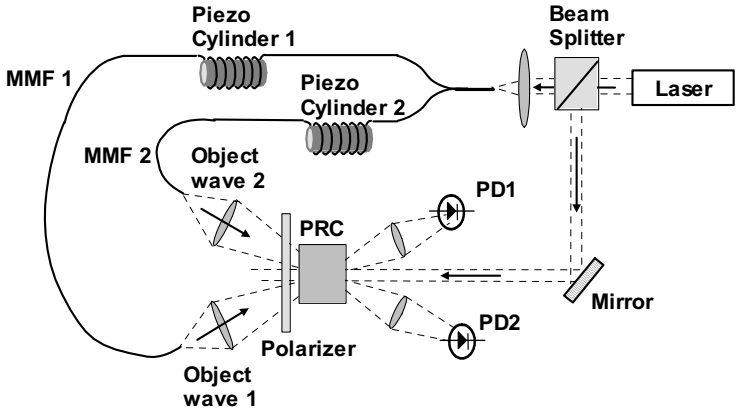

Fig. 4.4 Layout of the experimental setup for crosstalk measurements when only two measuring channels are incorporated in the sensor.

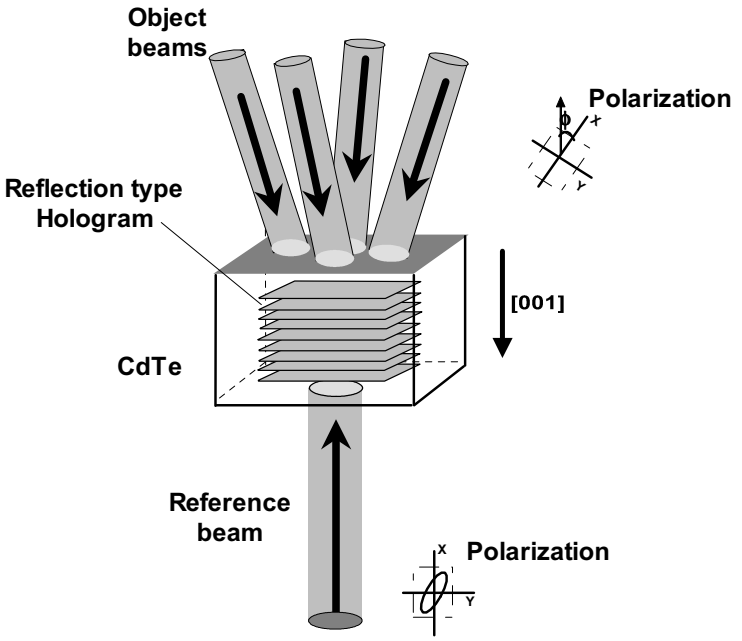

Fig. 4.5 Schematic of the multi wave interaction using the vectorial wave mixing in reflection geometry of hologram recording.

4.4 Crosstalk analysis.

As we have already mentioned above, the appearance of crosstalk in MTWM is mostly related to the photorefractive coupling between the different object waves. Therefore, it is obvious that by diminishing the efficiency of the wave coupling of the secondary holograms, we can diminish the crosstalk. The reference wave represents an additional illumination term which affects the visibility of the holograms recorded by the object-to-object interaction. Consequently, by increasing the intensity of the reference wave, we can decrease the visibility of secondary holograms, reducing the crosstalk.

In the configuration proposed in **Paper V**, the secondary holograms should not couple the object waves. However, we measured a small crosstalk. The experimental investigation revealed that the strongest physical reason for the crosstalk were the internal stresses in the PRC. Such an investigation was done by using the simplified experimental setup which uses only two measuring channels. We used the experimental setup similar to that one described in **Paper II,** whereas the sensor incorporated two separate MMFs with the same core diameter (550 μm) (see figure (4.4)). Each fiber was reeled on its respective piezoelectric cylinder. The two object and reference waves were focused in the same portion of the volume of the crystal's sample. When we applied sinusoidal voltage at the frequency *f* to any piezoelectric cylinders, we modulate the phase of the light transmitted through the respective fiber. This phase modulation causes the appearance of a harmonic signal at the same frequency *f* from the corresponding photodiode in the similar way, as reported in **Paper II**. After crossing the PRC, each object wave was focused on its respective photodetector. To estimate the crosstalk between the two measuring channels, we modulated the strains (at the frequency *f*) of only one fiber (the object wave 1) whereas we measured the response of the photodiode (PD2) corresponding to the other object wave emerging from the fiber which was non-excited. The measurements were done by means of a lock-in amplifier.

The response of the second photodiode at frequency *f* and *2f* was considered as a crosstalk which was evaluated by

$$\alpha_{S2} = \frac{|S_2(f)| + |S_2(2f)|}{|S_1(f)|} \tag{4.1}$$

We observed that when the object wave 1 was modulated at frequency *f* the PD2 detected both first and second harmonic of intensity modulation with the amplitude of first harmonic even bigger than the amplitude of second harmonic (see figure 4.6). In the following subsections, we explain the physical reasons for the appearance of the crosstalk.

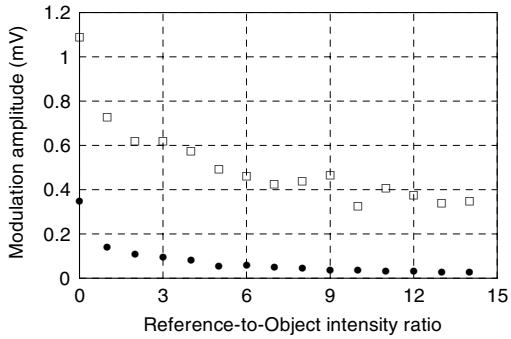

Fig. 4.6 Dependence of the signal from PD2 on the intensity ratio of the reference wave and the object wave 1. Measurements were carried out at the crystal area where the effect of stresses was the strongest. The periodical strains were excited in the fiber 1 at the frequency *f* so that the amplitude of the phase modulation of the object wave 1 is 1.1 radians. The object wave 2 had no modulation and its intensity at the crystal input was equal to that of the object beam 1. Squares are peak-to-peak modulation of the photocurrent at the frequency *f* and circles are the modulation amplitude at the frequency 2*f*.

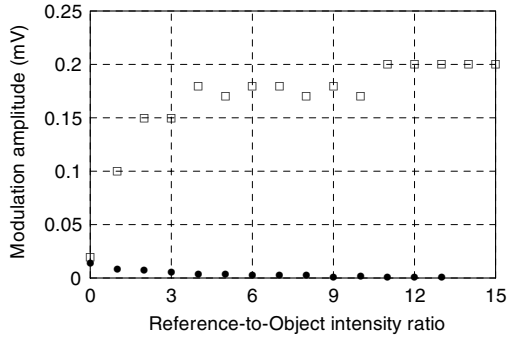

Fig. 4.7 Amplitude of the PD2-photocurrent modulation as a function of the reference-to-object waves intensity ratio measured in the crystal area where the effect of the internal stresses was the weakest. The other experimental parameters are the same as for measurements shown in figure (4.6). Squares are peak-to-peak modulation of the photocurrent at the frequency *f* and circles are the modulation amplitude at the frequency 2*f*.

4.4.1 Crosstalk due to coupling via transmission hologram

The main reason for the appearance of the crosstalk in our configuration is the presence of internal stresses in our particular sample of CdTe. The presence of the stresses was proved by placing the PRC between two crossed polarizers. When the sample was uniformly illuminated, there were portions of the crystal more transparent. The internal stresses may locally change the structure of the electrooptic tensor of the PRC, thus allowing the coupling of the object waves even if it is not allowed in our overall configuration. When the object wave 1 contains phase modulation with amplitude ϕ, its coupling with the object wave 2 having the same polarization state via the transmission hologram recorded in the diffusion regime results in quadratic phase demodulation

$$S_1(2f) = 2A_{tran.}\frac{I_{S1}I_{S2}}{I_R + I_{S1} + I_{S2}}\phi^2 \tag{4.2}$$

where $A_{\text{tran.}}$ is the proportionality coefficient of the transmission hologram which takes into account the crystal geometry, amplitude of the space-charge field, and the polarization states of the interacting waves(I_{S1} is the intensity of the object wave 1, I_{S2} the intensity of the object wave 2 and I_R intensity of the reference wave). The equation (4.2) shows that the object-to-object coupling leads to the appearance of the second harmonic of the PD2-photocurrent modulation whereas the reference beam just decreases the object-to-object beam coupling.

The appearance of the first harmonic relates with several physical reasons. One reason is the presence of stresses in the PRC. When the object waves travel in the crystal, the stresses may partially change the linear polarization state of each object wave to the elliptical, thus leading to linear phase demodulation owing the principle of VWM. Since the stresses are not uniformly distributed in the volume of the PRC, there will be portions of the crystal where their effect is stronger than in other portions. Such model was confirmed by executing two different measurements of the crosstalk in two different portions of the crystal's volume. One portion was that one where the effect of the internal stresses was the strongest (most transparent portion of the sample). The experimental curves which are shown in figure (4.6) represent the amplitude of first and second harmonic detected by PD2, when measurement were done in the portion where the effect of the stresses was the strongest, whereas the experimental curves which are shown in figure (4.7) represent the amplitude of first and second harmonic detected by PD2, when measurement were done in the portion where the effect of the stresses was the weakest. As one can see from figure (4.7), when the reference wave is absent the amplitudes for both second and first harmonic detected by PD2 are smaller in the second measurement.

4.4.2 Crosstalk due to scattering

Another mechanism which contributed to the crosstalk measured by PD2 is related to the light scattered from the object wave 1. Such a scattering appears due to the imperfections at the surface and/or in the volume of the photorefractive crystal. As we have seen in section (4.2), the presence of a polarizer results in the appearance of intensity modulation in the linearly polarized object wave. Since the intensity of such modulation manifests itself at same frequency f as the phase modulation, we measure a small signal at the same frequency from PD2 because of the scattered light. The intensity of the scattered light was detected when both the reference wave and object wave 2 were blocked. When the reference wave is switched on, it interferes with the scattered part of the first object wave thus recording a reflection-type hologram in the PRC. After being diffracted from this hologram, the reference beam is $\pi/2$-phase shifted in respect to the scattered part of the object wave 1 because both beams have different polarization states optimized by the VWM. Therefore, the phase modulation of the scattered part of the object wave 1 is linearly transferred into intensity modulation which is detected by the photodiode PD2. This explains the ten-fold increase of the modulation at the first harmonic shown in figure (4.6) and its independence from the presence of the object wave 2.

4.4.3 Intensity modulation of the reference wave

In **Paper V** we also present a third possible mechanism of the crosstalk which leads to the intensity modulation at the first harmonic. This third mechanism, which may occur even without direct object-to-object coupling or light scattering, relates to the intensity modulation of the reference wave. Such a modulation inevitably appears due to its coupling with the phase-modulated object wave 1. After diffraction from the diffusion hologram recorded by the object wave 1 and the reference wave, the latter is modulated at the first harmonic because of the fulfillment of the quadrature conditions owing the principle of VWM. However, the reference wave is also simultaneously diffracted in the direction of the photodiode PD2 by the second reflection-type hologram. Therefore, it contributes to the modulation of the PD2-photocurrent at the first harmonic.

The intensity of the modulated part of the reference wave diffracted from the first reflection hologram recorded with the object wave 1 is given as

$$S_1(f) = 2A_{refl.}\frac{I_R I_{S1}}{I_R + I_{S1} + I_{S2}}\phi \qquad (4.3)$$

where $A_{\text{refl.}}$ is the proportionality coefficient, which is different from $A_{\text{tran.}}$, because it describes the efficiency of a hologram of the reflection type. The amplitude of the intensity modulation of the reference wave $S_1(f)$ in equation (4.3) is exactly the same as the intensity modulation detected by the photodiode PD1, which is considered to be an informative signal. The intensity of the modulated part of the reference wave after diffraction from the second reflection hologram recorded with the object wave 2 is given as

$$S_2(f) = A_{refl.}^2 S_1(f) \frac{I_R I_{S2}}{(I_R + I_{S1} + I_{S2})^2} = 2A_{refl.}^3 \frac{I_R^2 I_{S1} I_{S2}}{(I_R + I_{S1} + I_{S2})^3} \phi \qquad (4.4)$$

The term $A_{refl.}^2 I_R I_{S2} / (I_R + I_{S1} + I_{S2})^2$ can be thought of as the diffraction efficiency of a single hologram. However, it includes the properties of the first and second interference pattern of the two reflection holograms. Such a term is zero when the reference wave is blocked, reaches its maximum at I_R/I_{S1} = 4, and decreases to zero for large values of the intensity ratio. However, in all measurements we observed only continuous decreasing or increasing of the first harmonic, as shown in experimental curves. Therefore, we supposed that in our sample of CdTe the contribution to the first harmonic of the crosstalk due to this last mechanism is negligible compared with the others

Chapter 5

Conclusions

This thesis presents three novel configurations for self-adaptive interferometers which are based on the (VWM) technique in a CdTe photorefractive crystal. In WVM the interfering light waves are mixed in the photorefractive crystal with different polarization states in order to achieve linear phase-to-intensity transformation in the diffusion-dominated mechanism (without external field). The wave mixing in a PRC records a dynamic hologram which acts as a self-adjusted combiner of both interfering waves, which allows only the fast phase transients of the object wave to be transformed into intensity modulation of the waves transmitted through the PRC. Moreover, the dynamic hologram is able to match the fronts of the reference wave with that of any speckled object wave and to compensate for both temporal and spatial instabilities in the intensity distribution of the object wave front. The properties of the dynamic hologram allow the MMF to be used as a sensitive element for measuring ultra-small displacements or deformations.

Usually, the photorefractive wave mixing is organized by using the transmission geometry of hologram recording. However, a strong electric AC-field has typically to be applied to enhance the wave coupling. Unfortunately, applying a strong external field to the PRC may be unacceptable for many practical applications. In this thesis, it is shown that the wave coupling in a self-adaptive holographic interferometer can be essentially improved by switching from transmission to reflection geometry of hologram recording in the PRC when it possesses enough concentration of photorefractive centers N_A. In experiments, two crystal samples with different concentrations of photorefractive centers were tested. In the reflection geometry, it was found that such an improvement was accompanied by a 4- to 5-fold increase of the interferometer relative detection limit for the sample BR-4Z-05 and a 1- to 5-fold increase for the sample BL-07-B1 compared with the best sensitivity which was found for the transmission geometry.

It is shown that the wave mixing in CdTe allows the achievement of high cutoff frequencies at relatively low intensities of interacting waves, due to the fast response time of the crystal. In experiments, cutoff frequencies of 300 Hz and 1250 Hz were measured for the BR-4Z- 05 and the BL-07-B1 samples, respectively, with a total optical intensity of interacting waves of 70 mW/cm^2. It is worth noting that cut-off frequencies higher than 1 kHz are required for industrial on-line applications. In spite of the fact that the hologram compensates for both temporal and spatial instabilities in the intensity distribution of the speckle pattern emerging from the fiber, it cannot compensate for instabilities in the polarization state of speckles of light emerging from the MMF. The MMF produces the largest source of noise affecting strain measurements when it is used as the sensitive element. However, this noise is significantly diminished by using a fiber with a larger core diameter. In this thesis, it has been shown that the 550 μm core fiber operates better as a strain

sensor than a fiber with a 50 μm core. The 11-fold increase of the core size led to a 5-fold reduction of the noise level. As a consequence, the dynamic range was increased from 17 to 30 dB. The obtained sensitivity allows a range measurement from 0.09 to 113 nm with a broadband of 50 MHz.

In this thesis it is shown that the orthogonal geometry of wave interaction in photorefractive CdTe crystal allows the linear detection of small phase shifts encrypted in a depolarized wave emerging from the MMF without any polarizing element. In experiments, when a depolarized wave was mixed in the PRC with an elliptically polarized reference wave, the rate of the phase-to-intensity transformation was 10% smaller than in the case of a linearly (vertically) polarized object wave. However, the absence of any polarizing element resulted in diminishing of the noise.

Classical TWM can be employed as a technique to multiplex several interferometers by using a single PRC [references]. However, such measuring systems are affected by appreciable crosstalk, which limits the sensitivity of each measuring channel. Moreover, a strong electric field has to be applied to the crystal to enhance the efficiency of the wave coupling. This thesis presents a novel configuration of a multiplexed self-adaptive interferometer that allows for simultaneous detection of dynamic strains excited in different multimode optical fibers. The multiplexing of adaptive interferometers is implemented in a single photorefractive crystal by using vectorial wave mixing in the reflection geometry of hologram recording without any external field. This configuration has potentially low crosstalk between the measuring channels. It is shown, that residual stresses and imperfections of particular photorefractive crystal of CdTe:V are the main reasons of the crosstalk in the proposed system. Nevertheless, it is possible to design a sensor consisting of 10 adaptive interferometers in the same volume of the crystal with a diminished dynamic band of measurements. Use of higher quality photorefractive crystals could improve the parameters of the multiplexed sensor.

Chapter 6

Summary of publications

The main goal of our studies was the implementation and optimization of fiber-optic interferometers for the detection of ultra-small mechanical vibrations. All the sensors presented in this thesis use multimode optical fibers as sensitive elements. In our sensors, the mechanical vibrations induce phase shifts of highly coherent light traveling through the fiber. The detection of those phase shifts is done by employing self-adaptive holographic interferometers which are implemented by using the vectorial wave mixing in a CdTe photorefractive crystal.

The vectorial wave mixing involves mixing of the reference and object waves with different polarization states. By choosing the proper orientation of the hologram in the crystal and the polarization state for both the object and reference wave, we can achieve the highest detection limit in the linear regime of the phase demodulation. We have analyzed the vectorial wave mixing for different geometries of hologram recording. In all our papers we show the performance of the pure diffusion regime of hologram recording.

The pure diffusion regime of hologram recording prevents the application of a strong electric field to the crystal, which may be unacceptable for many practical applications. Traditionally, by applying an ac-field it is possible to obtain higher amplitude of the space charge field in the crystal than in the case of a pure diffusion regime of hologram recording. In **Papers I, III and IV** we have shown that by employing the reflection geometry instead of the transmission geometry of hologram recording we can enhance the amplitude of the space charge field even without applying an external electric field. By enhancing the amplitude of the space charge field, we increase the coupling constant, thus resulting in better efficiency of the phase demodulation.

In **Papers I , III and IV** we have also demonstrated that the high cut-off frequency of the interferometer achieved by using low-power light sources due to fast response of CdTe crystal allows the elimination of temperature fluctuations and other industrial noises.

In **Paper II** we have presented an interferometric sensor for sensing dynamic strains of multimode optical fiber caused by mechanical vibrations. Such a sensor is the first to use grating recording without applying any external field, which was made possible by the fact that it uses the reflection geometry of hologram recording. During our experiments we discovered that the largest source of noise in the dynamic-strains sensor with multimode fiber is the polarization instability of the dynamic speckle pattern emerging from the fiber. Due to its nature, we called it polarization noise. In the sensor presented in **Paper II,** the presence of polarization filtering at the fiber output is a necessary requirement for the achievement of linear phase demodulation. Therefore, the polarization

noise is inevitable**.** At same time, in **Paper II** we have experimentally demonstrated that using a fiber with a thicker core leads to diminishing of the polarization noise. Consequently, use of fiber with the thicker core enables the detection of smaller fiber strains. Experimental results on the polarization noise have also been studied in **Papers III and IV.**

In **Paper VI** we have proposed a configuration of a fiber optic sensor which has been implemented by using the vectorial wave mixing in the orthogonal geometry of hologram recording. The orthogonal geometry of wave mixing enables the linear detection of phase shift even from completely depolarized waves without using any polarizer filtering. The absence of polarizer filtering at the fiber output results in strong diminishing of the polarization noise.

In **Paper VII** we use the theory of vectorial wave coupling to explain the results obtained in **Paper VI.** Moreover, we compare the orthogonal geometry with the transmission and reflection geometries.

In **Paper V** we have proposed a scheme of sensor multiplexing which uses the VWM reflection geometry of hologram recording. The main feature of this configuration is the low crosstalk between measuring channels. The low crosstalk level relates to the crystal orientation in our configuration. In **Paper V** we have presented a detailed description of the physical mechanisms which lead to the appearance of the very small crosstalk between the measuring channels.

References

[1] H. J. Eichler, P. Günter, and D W. Pohl , "Laser-Induced Dynamic Grating, " (Springler-Verlag, Berlin, 1986).

[2] P. Günter and J. P. Huignard, "Photorefractive Materials and Their applications I and II," (Springler-Verlag, Berlin, 1988).

[3] P. Yeh, "Introduction To Photoreractive Non Linear Optics," (Wiley & Sons, New York, 1993).

[4] A. Ashkin, G. D. Boyd, J. M. Dziedzic, R. G. Smith, A. A. Ballman, J. J. Levinstein, and K. Nassau, "Optically induced refractive index inhomogeneities in $LiNbO_3$ and $LiTaO_3$," Appl. Phys. Lett. **9**, 72-74, (1966).

[5] E. S. Maniloff and K. M. Johnson, "Maximized photorefractive holographic storage," J. Appl. Opt. **70**, 4702-4707 (1991).

[6] H. Sasaki, Y. Fainman, J. E. Ford, Y. Taketomi, and S. H. Lee, "Dynamic photorefractive optical memory," Opt. Lett. **16**, 1874-1876, (1991).

[7] D. Z. Anderson, D. M. Lininger, and J. Feinberg, "Optical tracking novelty filter," Opt. Lett. **12**, 123-125, (1987).

[8] Y. Fainman, C.C. Guest, and S. H.Lee, "Optical digital logic by two beam coupling in photorefractive materials,"Appl. Opt. **25,** 1958-1603, (1986).

[9] A. A. Kamshilin and M. P. Petrov, "Holographic image conversion in a $Bi_{12}SiO_{20}$ crystal," Soviet Techonologies Physics letters **6,** 144-207, (2002).

[10] S. I. Stepanov, "Application of photorefractive crystals," Rep. Prog. Phys. **57**, 39-116, (1994).

[11] I. M. Rossomakhin and S. I. Stepanov, "Linear adaptive interferometers via diffusion recording in cubic photorefractive crystals," Opt. Commun. **86**, 199-204, (1991).

[12] R. K. Ing and J.-P. Monchalin, "Broadband optical detection of ultrasound by two-wave mixing in a photorefractive crystal," Appl. Phys. Lett. **59**, 3233-3235, (1991)

[13] N. V. Kukhtarev, V. B. Markov, S.G. Odulov, M. S. Soskin, and V. L. Vinetskii, "Holographic storage in electrooptic crystals. I. Steady state," Ferroelectrics **22**, 949-960, (1979).

[14] A. Blouin and J.-P. Monchalin, "Detection of ultrasonic motion of a scattering surface by two-wave mixing in a photorefractive GaAs crystal, " Appl. Phys. Lett. **65**, 932-934, (1994).

[15] B. Campagne, A. Blouin, L. Pujol, and J.-P. Monchalin, "Compact and fast response ultrasonic detection device based on two-wave mixing in a gallium arsenide photorefractive crystal," Rev. Sci. Instrum. **72**, 2478-2482, (2001).

[16] B. I. Sturman, M. Mann, E. V. Podivilov, K. H. Ringhofer, E. Shamonina, V. P. Kamenov, E. Nippolainen, V. V. Prokofiev, and A. A. Kamshilin, "Theory of photorefractive vetorial wave coupling in cubic crystal," Phys. Rev. E **60**, 3332-3352, (1999).

[17] S.I. Stepanov, and M.P. Petrov, "Efficient unstationary holographic recording in photorefractive crystal under an external alternating electric field," Opt. Comm. **53**, 292-295, (1985).

[18] S.I. Stepanov, M.P. Petrov, "Nonstationary holographic recording for efficient amplification and phase conjugation," Proc. ICO-13, Sapporo, 1984.

[19] Y. V. Miklyaev and V. I. Safonov, "Recording of photorefractive holograms by an AC field perpendicular to the grating vector," Pure Appl.Opt., **5**, 445-451, (1996).

[20] A. Yariv, and P. Yeh, "Optical waves in crystals," (J. Wiley & Sons, New York, 1984).

[21] B. Guru, and H. Hiziroğlu, "Electromagnetic field theory fundamentals," (Cambridge University Press 2004).

[22] L. Solymar, D. J. Webb, and A. Grunnet-Jepsen, "The physics and applications of the photorefractive materials," (Clarendon Press Oxford, 1996).

[23] J. P. Huignard and A. Marrakchi, "Two wave mixing and energy transfer in $Bi_{12}SiO_2$, " Opt. Lett. **6**, 622, (1981)

[24] F. M. Davidson, L. Boutsikaris, and M. A. Krainak, "Coherent optical detection through two wave mixing photorefractive materials," Opt. Lett. **13,** 506-508, (1988).

[25] E. Shamonina, K. H. Ringhofer, B. I. Sturman, G. Cedilnik, A. Kießling, R. Kowarschik, A. A. Kamshilin, V. V. Prokofiev,and T. Jaaskelainen, "Giant momentary readout by switching electric fields during two wave mixing insillenites," Opt. Lett., **23**, 1435-1437, (1998).

[26] A. Marrakchi, R.V. Johnson, and A.R. Tanguay,"Polarization properties of photorefractive diffraction in electrooptic and optically active sillenite crystals (Bragg regime)," J. Opt. Soc. Am. B 3, 321-336, (1986).

[27] S. Mallick, D. Roue`de, and A.G. Apostolidis, "Efficient and polarization characteristics of phootrefractive diffraction in a $Bi_{12}SiO_{20}$," J. Opt. Soc. Am.B, **4**, 12471259, (1987).

[28] A. Brignon and K.H. Wagner, "Polarization state evolution and eigenmode switching in photrefractive BSO," Opt. Comm., **101**, 239-246, (1993).

[29] B.I. Sturman, D.J. Webb, R. Kowarschik, E. Shamonina, and K.H. Ringhofer, "Exact solution of he Bragg-diffraction problem in sillenites," J. Opt. Soc. Am. B **11**, 1813-1819, (1994).

[30] B.I. Sturman, O. S. Filippov, “Solutions for vectorial beam coupling under ac field in cubic photorefractive crystals,” Phys. Rev. **E 68**, 036613 (2003) [10 pages].

[31] G. Doswell, and H. Kunov, “Active stabilization system for a laser interferometer,” Rev. Sci. Instrum., **61 ,** 1986-1987, (1990).

[32] J. W. Wagner and J. B. Spicer, “Theoretical noise-limited sensitivity of classical interferometry,” J. Opt. Soc. Am. B, **4**, 1316-1326, (1987).

[33] S.I. Stepanov, “International trends in Optics,” (J. W. Goodman Accademic New York, 1991).

[34] S. I. Stepanov, “Applications of photorefractive crystals,” Rep. Prog. Phys. **57** (1994).

[35] R. J. Collier, C. B. Burckhardt, and L. H. Lin, “Optical Holography, ” (Academic Press, New York, 1971)

[36] T. J. Hall, M. A. Fiddy and M. S. Ner,. “Detector for an optical-fiber acoustic sensor using dynamic holographic interferometry," Opt. Lett. **5**, 485-488 (1980).

[37] P. Delaye, A. Blouin, D. Drolet, L.-A. de Montmorillon, G. Roosen, and J.-P. Monchalin, “Detection of ultrasonic motion of a scattering surface using photorefractive InP:Fe under an applied dc field,” J. Opt. Soc. Am. B **14**, 1723-1734, (1997).

[38] I. M. Rossomakhin and S. I. Stepanov, “Linear adaptive interferometers via diffusion recording in cubic photorefractive crystals,” Opt. Comm., **86**, 199-204, (1991).

[39] B. Campagne, A. Blouin, L. Pujol, and J.-P. Monchalin, “Compact and fast response ultrasonic detection device based on two-wave mixing in a gallium arsenide photorefractive crystal, ” Rev. Sci. Instrum., **72**, 2478-2482, (2001).

[40] A. A. Kamshilin and A. I. Grachev, “Adaptive interferometer based on wave mixing in photorefractive crystal under alternating electric field, ” Appl. Phys. Lett., **81**, 2923-2925, (2002).

[41] J. W. Wagner and J. Spicer, “Theoretical noise limited sensitivity of classical interferometry,” Opt. Soc. Am. B **4**, 1316-1326 (1987).

[42] L.-A de Montmorillon, P. Delaye, J.-C Launay, and G. Roosen, J. Appl. Phys., “Novel theoretical aspects on photorefractive ultrasonic detection and implementation of a sensor with a optimum sensitivity,” **82**, 5913 (1997)

[43] I. L. Bershtein, “Measurement of extremely small changes of path difference of two light oscillations,” Dokl. Acad.Nauk., USSR **94**, 655, (1954).

[44] R. L. Forward, "Wideband laser-interferometer graviational-radiation experiment," Phys. Rev. **D 17**, 379-390, (1978).

[45] M. P. Petrov, S. I. Stepanov, and A. V. Khomenko, "Photorefractive crystals in coherent optical systems," (Springer-Verlag, Berlin, Germany, 1991).

[46] K.T.V. Grattan , Dr. T. Sun, "Fiber optic sensor technology: an overview," Sensors and Actuators, **82** pp.40-61.(2000).

[47] D. A. Jackson and J. D. C. Jones, "Fibre optic sensors," Opt. Acta. **33,** 1469-1503 (1986).

[48] W. J. Bock, A. W. Domafiski, and Tomasz R. Wolifiski, "Influence of high hydrostatic pressure on beat length in highly birefringent single-mode bow tie fibers," Appl. Opt. **29**, 3484-348, (1990).

[49] A. Bertholds and R. Dandliker, "High-resolution photoelastic pressure sensor using low birefringence fiber," Appl. Opt., **25**, 340-343, (1986).

[50] E. J. Friebele, M. A. Putnam, H. J. Patrick, A. D. Kersey, A. S. Greenblatt, G. P. Ruthven, M. H. Krim, and K. S. Gottschalck, "Ultrahigh-sensitivity fiber-optic strain and temperature sensor," Opt. Lett., **23**, 222-224, (1998)

[51] A. A. Kamshilin, T. Jääskeläinen, A. V. Khomenko, and A. Garcia-Weidner, "Multimode fiber optic sensor using photorefractive double phase conjugator," Appl. Phys. Lett., **67,** 2585-2587, (1995).

[52] N. S.-K. Kwong, "Fiber-optic sensor using a tandem combination of a multimode fiber and a self-pumped phase conjugator," Opt. Lett., **14,** 590-592, (1989).

[53] T. W. Murray, H. Tuovinen, and S. Krishnaswamy, "Adaptive optical array receivers for detection of surface acoustic waves," Appl. Opt., **39,** 3276-3284 (2000).

[54] T. W. Murray and S. Krishnaswamy, "Multiplexed interferometer for ultrasonic imaging applications," Opt. Eng., **40,** 1321-1328, (2001).

[55] P. A. Fomitchov, T. W. Murray, and S. Krishnaswamy, "Intrinsic fiber-optic ultrasonic sensor array using multiplexed two-wave mixing interferometry," Appl. Opt. **41,** 1262-1266, (2002).

Kuopio University Publications C. Natural and Environmental Sciences

C 238. Pinto, Delia M. Ozonolysis of constitutively-emitted and herbivory-induced volatile organic compounds (VOCs) from plants: consequences in multitrophic interactions.
2008. 110 p. Acad. Diss.

C 239. Berberat neé Kurkijärvi, Jatta. Quantitative magnetic resonance imaging of native and repaired articular cartilage: an experimental and clinical approach.
2008. 90 p. Acad. Diss.

C 240. Soininen, Pasi. Quantitative ^{1}H NMR spectroscopy: chemical and biological applicatons.
2008. 128 p. Acad. Diss.

C 241. Klemola, Kaisa. Cytotoxicity and spermatozoa motility inhibition resulting from reactive dyes and dyed fabrics.
2008. 67 p. Acad. Diss.

C 242. Pyykönen, Teija. Environmental factors and reproduction in farmed blue fox (Vulpes lagopus) vixens.
2008. 78 p. Acad. Diss.

C 243. Savolainen, Tuomo. Modulaarinen, adaptiivinen impedanssitomografialaitteisto.
2008. 188 p. Acad. Diss.

C 244. Riekkinen, Ossi. Development and application of ultrasound backscatter methods for the diagnostics of trabecular bone.
2008. 79 p. Acad. Diss.

C 245. Autio, Elena. Loose housing of horses in a cold climate: effects on behaviour, nutrition, growth and cold resistance.
2008. 76 p. Acad. Diss.

C 246. Saramäki, Anna. Regulation of the p21 (CDKNIA) gene at the chromatin level by 1 alfa,25-dihydroxyvitamin D3.
2008. 100 p. Acad. Diss.

C 247. Tiiva, Päivi. Isoprene emission from northern ecosystems under climate change.
2008. 98 p. Acad. Diss.

C 248. Himanen, Sari J. Climate change and genetically modified insecticidal plants: plant-herbivore interactions and secondary chemistry of Bt Cryl Ac-Toxin producing oilseed rape (Brassica napus L.) under elevated CO2 or O3.
2008. 42 p. Acad. Diss.

C 249. Silvennoinen, Hanna. Nitrogen and greenhouse gas dynamics in rivers and estuaries of theBothnian Bay (Northern Baltic Sea).
2008. 98 p. Acad. Diss.

C 250. Degenhardt, Tatjana. An integrated view of PPAR-dependent transcription.
2009. 120 p. Acad. Diss.

C 251. Häikiö, Elina. Clonal differences of aspen (Populus spp.) in responses to elevated ozone and soil nitrogen.
2009. 49 p. Acad. Diss.

C 252. Hassinen, Viivi H. Search for metal-responsive genes in plants: putative roles in metal tolerance of accumulation.
2009. 84 p. Acad. Diss.